THE ASTROPHYSICAL JOURNAL, 465:96–114, 1996 July 1

STELLAR AND GASEOUS KINEMATICS OF SEYFERT GALAXIES. II. THE ROLE OF THE BULGE

CHARLES H. NELSON[1] AND MARK WHITTLE
Astronomy Department, University of Virginia, Charlottesville, VA 22903
Received 1995 October 5; accepted 1996 January 23

ABSTRACT

We have used measurements of the nuclear stellar velocity dispersion, σ_*, for a large sample of Seyfert galaxies to investigate the role played by the nuclear gravitational potential in defining the properties of active galaxies. We address four basic questions. First, do Seyferts have unusual nuclear stellar dynamical properties compared to those of normal galaxies? Second, what are the relative contributions of gravitational and nongravitational forces creating the velocity field of the nuclear emission-line gas? Third, how do the emission-line and radio luminosities in the narrow-line region (NLR) depend on the bulge potential? Fourth, in what way are the properties of Seyfert galaxies related to those of radio galaxies?

We find that Seyferts define a tight correlation between σ_* and bulge absolute magnitude, similar to the Faber-Jackson relation for normal spiral bulges. We infer from this that Seyfert bulges are kinematically normal. The Seyfert relation is, however, offset to higher bulge luminosities, which we interpret as evidence for a lower mean mass-to-light ratio. Either Seyferts have experienced higher than average star formation or they avoid systems with older stellar populations. We analyze the relations between σ_* and both galaxy rotation and galaxy absolute magnitude, finding similar relations to those of normal spirals. This also supports a normal kinematic relation between bulges and disks in Seyferts.

A moderately strong correlation between σ_* and [O III] profile width suggests that gravitational motion plays an important role in the NLR velocity field. The correlation is weaker with [O III] base and wing widths, although the interpretation of this is not yet clear. The remaining real scatter on the relations indicates the importance of other factors. In particular, objects with kiloparsec-scale linear radio sources can have significantly broader [O III] lines, confirming that interaction with an expanding radio source can accelerate the NLR gas. We also find that Seyferts that are tidally distorted have broader [O III] lines. The kinematic relations do not depend on galaxy inclination or Seyfert class, suggesting that the NLR gas is confined neither to the plane of the galaxy nor to the plane of an inner obscuring disk.

We find moderately strong correlations between [O III] luminosity and σ_* and between radio luminosity and σ_*, confirming the importance of the bulge potential in determining the overall NLR luminosity. More massive bulges may have more massive black holes, provide more fuel through stellar mass loss, allow larger emitting regions, and/or have higher pressures and emissivities.

We included radio galaxies in our analysis of the correlation between radio luminosity and bulge mass. Using total radio luminosity, the radio galaxies and Seyferts show little connection. However, when the core luminosities of radio galaxies are used, the two groups form a single continuous steep relation spanning 6 mag in $M_{\rm bul}$. There is some evidence that at a given bulge mass, more "jetlike" sources (Seyferts with linear morphology, and cores of FR II radio galaxies) are more luminous than the less "jetlike" sources (Seyferts without linear morphology, and cores of FR I radio galaxies). Finally, the radio galaxies fall on the same Faber-Jackson relation as the Seyferts, offset from the normal galaxy relation. Thus, we see both unity and continuity between the properties of Seyfert galaxies and radio galaxies. In particular, we can understand the separation of radio-quiet and radio-loud objects into spirals and ellipticals as a direct manifestation of a more fundamental dependence of galactic scale radio luminosity on bulge mass.

Subject headings: galaxies: kinematics and dynamics — galaxies: Seyfert — radio continuum: galaxies

1. INTRODUCTION

In our first paper (Nelson & Whittle 1995, hereafter Paper I), we presented measurements of the nuclear stellar velocity dispersion for a large sample of Seyfert galaxies. This parameter, perhaps more than any other, characterizes the depth of the nuclear gravitational potential on scales $\sim 10^2$–10^3 pc. Our motivation is to study the nuclear potentials of Seyferts to find out whether they differ from those of normal galaxies and whether they influence in any way the properties of the active regions.

In the past, most work on Seyfert galaxies has focused on their active properties, leading to a fairly detailed understanding of the physical processes operating within the nucleus. Here, however, we emphasize the nature of the host galaxy and in particular the nature of the bulge. There is already considerable evidence that the properties of the bulge influence both the onset and character of nuclear activity. The obvious fact that galactic activity always

[1] Current address: Space Telescope Science Institute, 3700 San Martin Drive, Baltimore, MD 21218.

occurs in the nuclear regions points to the importance of a deep potential in the generation of activity. The preference of Seyferts to inhabit relatively luminous early-type spirals suggests that not only the presence of a bulge but also its mass is important. More recent work has explored the connection between the host galaxy properties and the properties of the narrow-line region (NLR), with results suggesting that both the NLR velocity field and its radio and emission-line luminosities depend on the bulge mass and hence on the nuclear gravitational field.

In most of these earlier studies, the parameters chosen to characterize the host galaxy have been only indirectly linked to the nuclear gravitational field. For example, near-nuclear magnitude, bulge magnitude, H I line width, CO line width, and optical rotation amplitude have all been used in correlation studies with NLR line width parameters (see, e.g., Busko & Steiner 1989; Heckman et al. 1989; Veilleux 1991a, b; Whittle 1992a, b, c, hereafter W92a, b, c). The next important step is to use nuclear stellar velocity dispersions, σ_*, as a more direct probe of the inner gravitational field. So far, comparatively few measurements of σ_* have been made for Seyferts. Those studies that have been done support the importance of gravity in the NLR and suggest that they are kinematically normal (Wilson & Heckman 1985; Terlevich, Diaz, & Terlevich 1990). Our work expands considerably on these two earlier studies.

While in Paper I we present measurements of stellar and gaseous kinematics for a sample of $\sim$80 active galaxies, in this paper we use these measurements for a kinematic study. In § 2 we briefly review Paper I and describe the statistical methods used in the present paper. In § 3 we compare the kinematics of Seyferts and normal galaxies by considering the relationships between the stellar velocity dispersion, the bulge absolute magnitude, and the galaxy rotation amplitude. In § 4 we investigate the gravitational and non-gravitational nature of the NLR velocity field by considering the relationship between the stellar velocity dispersion and a number of parameters characterizing the [O III] λ5007 emission-line width. In § 5 the relationship of radio and emission-line luminosities to bulge mass is explored. In § 6 we look for continuity between the Seyferts and radio galaxies to explore similarities between radio-quiet and radio-loud active galactic nuclei (AGNs). Finally, in § 7 we summarize our conclusions.

2. SAMPLE AND METHODS

In Paper I, we presented measurements of the stellar and gaseous kinematics for a sample of $\sim$75 Seyfert galaxies. Two wavelength regions were used, one centered on the Ca II triplet ($\sim$8550 Å) and the other on Mg *b* ($\sim$5175 Å). We derived nuclear stellar velocity dispersions, σ_*, systemic velocities, V_*, and their errors using a cross-correlation analysis similar to that developed by Tonry & Davis (1979). These methods were tested using simulated galaxy spectra and were found to give reliable values and errors for σ_* for S/N ratios and line widths spanning the range found for our data. Furthermore, comparison of Ca II triplet, Mg *b*, and published values for σ_* gave good agreement within the estimated errors. In addition, line widths and redshifts for the [O III] λ5007 and [S III] λ9069 emission lines were also measured. Final values of both gas and star kinematic parameters were obtained by combining our measurements with previously published values. We also assigned quality ratings to indicate the reliability of the measurements. These are used for screening data in the analysis and are intended to reflect difficulties in the measurements not explicitly accounted for in the formal errors. Data qualities a, b, c, and r indicate reliable values, less reliable but adequate values, poor values, and rejected values respectively.

Several additional parameters related to the properties of the host galaxy are used in our analysis. These are tabulated and described in more detail in Paper I and W92a. Briefly, they include absolute total and bulge *B* magnitudes, $M_{\rm tot}$ and $M_{\rm bul}$, with corrections for internal and galactic extinction, nonstellar light, and the effects of redshift; and the maximum rotation amplitude of the galaxy, $\Delta V^c_{\rm rot}$, as derived from H I widths and galaxy rotation curves, corrected for inclination, *i*. Radio morphologies for each object have been compiled as follows: L = linear, D = diffuse, A = ambiguous, U = unresolved, and S = slightly resolved. The parameters DC and IAC, reflect the degree of morphological disturbance and the proximity of neighboring galaxies on a scale of 1 to 6. The parameter PC is the maximum of these two. In § 5, parameters related to the activity in the nucleus are used, including the radio luminosity at 1415 MHz, L_{1415}, and the [O III] emission-line luminosity, L_{5007}. All parameters related to luminosity in this paper have been calculated assuming $H_0 = 50$ km s^{-1} Mpc^{-1} and $q_0 = 0$.

Throughout this paper we use a number of statistical techniques to examine relationships between two or three variables. Since formal errors are not always available, we cannot weight the data points by their uncertainties, and we instead use our data quality ratings, described above, to exclude lower quality data from the analysis. To assess correlation strength, we use the Pearson linear correlation coefficient, $R_{\rm P}$, and its associated two-tail probability of no correlation, *P*(null). We also make use of nonparametric statistics: the Spearman rank correlation coefficient, $R_{\rm S}$, and the Kendall rank correlation parameter $Z_{\rm K}$, which gives the probability of rejecting the null hypothesis expressed in standard deviations. Linear fits to two variable correlations are presented as either the bisector (OLS bisector) or the mean (OLS mean) of ordinary least-squares regressions minimized in each variable (Isobe et al. 1990). The OLS bisector method is considered to give the more reliable results when the uncertainties in each variable are large; however, the OLS mean is more commonly used. To test for the presence of a third variable, we use partial linear and rank correlation coefficients. Multiple linear regression is used to derive the dependence of one variable on the other two. We also use the Kolmogorov-Smirnov (K-S) test to determine the likelihood that two distributions are drawn from the same parent population, Student's *t*-test to compare the means of two distributions, and the *F*-test to compare variances.

3. RELATIONS BETWEEN VIRIAL PARAMETERS: σ_*, $\Delta V^c_{\rm rot}$, AND $M_{\rm bul}$

In this section we explore the relationships between the nuclear stellar velocity dispersion, σ_*, the full galaxy rotation amplitude corrected for inclination, $\Delta V^c_{\rm rot}$, and the bulge absolute magnitude in the *B* band, $M_{\rm bul}$. Each of these parameters probes the galaxy gravitational field in a different manner, and the relationships between them reflect the particular properties of each galaxy, such as the mass-to-light ratio, the form of the stellar velocity field, and the mass distribution. Differences between these relations for

Seyferts and normal galaxies may reveal factors that are important to the presence and evolution of the active nucleus.

Since surface photometry is not yet available for our sample galaxies, bulge magnitudes have been derived from published total magnitudes, M_{tot}, by applying a correction for disk light, Δm_{bul}, which is a simple function of Hubble type, T (Simien & de Vaucouleurs 1986). A correction, Δm_A, has also been applied to account for the continuum and line emissions from the active nucleus. These corrections have been described in greater detail in W92a.

The galaxy rotation amplitudes are taken from measured rotation curves or H I profiles and are corrected for the inclination of the galaxy. For H I, the measurements are generally taken as the full width of the profile at 20% of the peak height. Rotation amplitudes derived from rotation curves are the full velocity difference across the diameter of the galaxy. These parameters have been shown to be equal for most normal galaxies, and if both are of suitable quality, they are combined to yield ΔV^c_{rot}.

3.1. *The Faber-Jackson Relation for Seyfert Galaxies: σ_* versus M_{bul}*

The physical properties of elliptical galaxies and the bulges of spiral galaxies can be described by a three-parameter system that includes σ_*, M_{bul}, and the mean surface brightness, $\langle\mu\rangle$. Spheroidal stellar systems occupy a plane in the space defined by these three parameters, often referred to as the "fundamental plane" (Djorgovski & Davis 1987; Dressler et al. 1987; Bender, Burstein, & Faber 1992). Early work on the structure and dynamics of spheroids focused on a projection of the fundamental plane, namely the correlation between σ_* and M_{bul}, known as the Faber-Jackson (F-J) relation, often written as $L \propto \sigma_*^n$, where $n \sim 3$–4.

Figure 1*a* shows the $L \propto \sigma_*^n$ relation for Seyferts. Here we plot FWHM$_*$($=2.35 \times \sigma_*$) against M_{bul} showing a tight correlation ($R = -0.72$, $Z_K = -6.07$; throughout this work, we use FWHM$_*$). In Figure 1*a*, we exclude objects with the worst bulge magnitude qualities, f. (Because of the Hubble type dependence of the bulge magnitude, its quality rating is a combination of the total magnitude and the Hubble type qualities and so extends from a to f; see W92a.) We note that the results are not significantly changed by raising the data quality cutoffs.

The solid line in Figure 1*a* shows a fit to the data using the OLS mean regression method (see § 2), yielding an exponent $n = 2.7 \pm 0.3$ for the $L \propto \sigma_*^n$ relation, and a zero point FWHM$_*(-20) = 285 \pm 8$ km s^{-1}, where FWHM$_*(-20)$ is FWHM$_*$ at $M_{bul} = -20$. The tight correlation is gratifying confirmation of the reliability of the velocity dispersion measurements presented in Paper I. The scatter measured parallel to the log σ_* axis is 0.1, not much greater than the mean error on log σ_* of ± 0.07.

At this stage, it is useful to examine the influence of magnitude corrections on the M_{bul} versus σ_* diagram, in particular corrections due to nuclear nonstellar light and corrections for disk light. Our purpose is to verify that these

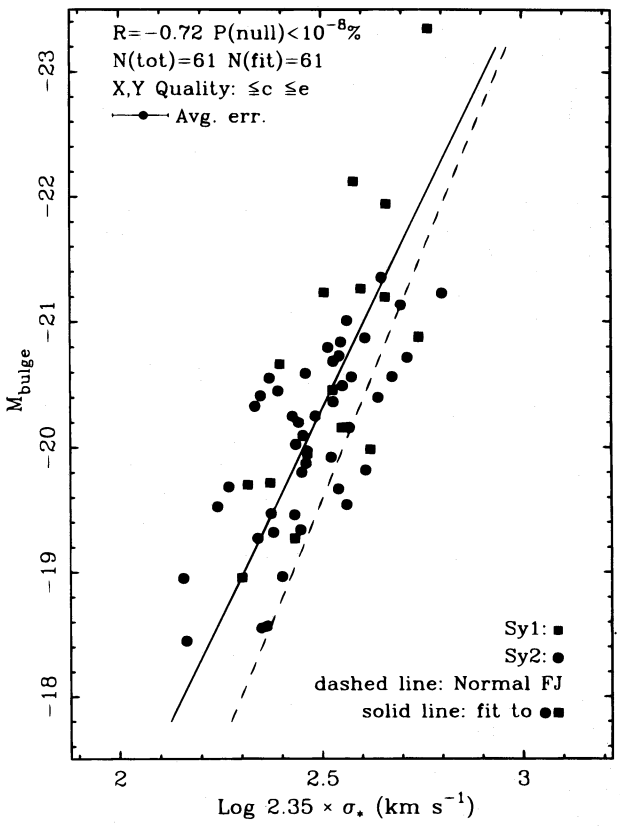

FIG. 1*a*

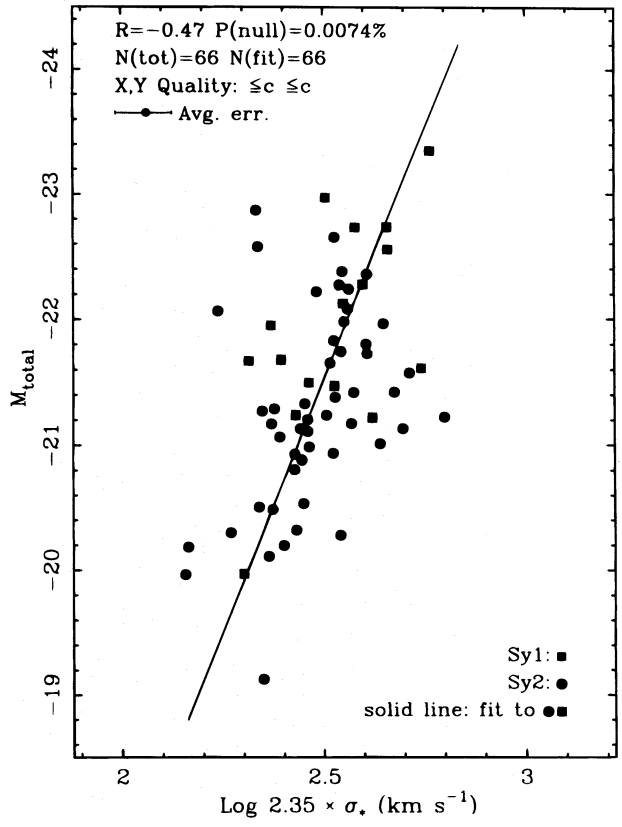

FIG. 1*b*

FIG. 1.—(*a*) Faber-Jackson relation for Seyfert galaxies using *B*-band bulge magnitudes is plotted. The solid line shows the fit using the OLS mean regression. The dashed line shows the $L \propto \sigma_*^n$ relation for normal galaxies derived by Whittle (1992c) for a sample of 243 normal galaxies. The mean error bar for σ_* is shown in the upper left. (*b*) Total *B* absolute magnitude vs. σ_* for Seyfert galaxies is shown. Note the greater scatter and decreased correlation strength compared with the M_{bul} vs. σ_* relation shown in (*a*). Here, the *Y*-axis scale has been shifted by 1 mag relative to (*a*).

corrections have not introduced any spurious or systematic effects.

The correction for the nonstellar luminosity of the active nucleus is generally small ($\langle \Delta m_A \rangle = 0.04$) but can be large for a few objects. Excluding those objects for which the active correction is greater than 0.1 mag (and so have perhaps more uncertain M_{bul} values) does not significantly change the correlation strength ($R = -0.74$, $Z_K = -5.7$, for the 53 remaining objects) or the fit. Excluding the correction for active contributions altogether has, again, almost no effect ($R = -0.72$, $Z_K = -6.2$). This is perhaps not surprising, since our sample is limited to Seyferts with relatively weak nonstellar contribution so that the stellar absorption features remain strong enough to measure.

The correction for disk light assumes that the bulge-to-disk ratio (B/D) in Seyfert galaxies has the same dependence on Hubble type as in normal galaxies. Since Δm_{bul} is solely a function of Hubble stage, T, we can test its effectiveness using partial correlation analysis of M_{tot}, σ_*, and T (here we follow the analysis of M_{tot}, [O III] FWHM, and T given in W92c). First, as shown in Figure 1*b*, the relation between σ_* and M_{tot} is more scattered ($R = -0.44$, $Z_K = -4.0$) than the one between σ_* and M_{bul} ($R = -0.72$, $Z_K = -6.07$), showing that it is the bulge mass, not the total galaxy mass, that is preferentially linked to σ_*. Second, the partial correlation strength at fixed T is considerably stronger ($R_{M_{tot},\sigma}|_T = -0.64$, $Z_K|_T = -5.8$), confirming that it is Hubble type, and therefore B/D ratio, which is a key parameter in accounting for the scatter on the M_{tot} versus σ_* relation.

Finally, if the B/D ratio in Seyferts is essentially normal, we would expect the scatter on the σ_* versus M_{tot} plot to have the same dependence on Hubble type as Δm_{bul}. A multiple linear regression assuming M_{tot} to be the dependent variable gives

$$M_{tot} = -10.812(\pm 1.606) - 4.192(\pm 0.639) \log (\mathrm{FWHM}_*) - 0.191(\pm 0.033) \times T \quad (1)$$

for the best fit using galaxies with Hubble type qualities b or better. Interestingly, the same analysis applied to a sample of normal galaxies gives -0.20 for the coefficient on T (W92c), which suggests a strong kinematic similarity between Seyfert and normal galaxies.

We next plot in Figure 2 the residuals of the M_{tot} versus σ_* relation (minimized in ΔM_{tot}) against Hubble type. The right-hand Y-axis gives the value of ΔM_{tot}, and the dashed line shows a linear fit to the data, the slope of which simply reproduces the coefficient on T in equation (1). The left-hand Y-axis gives the value of Δm_{bul} where we have defined Δm_{bul} to be zero at $T = -5$, i.e., we assume that ellipticals have no disk contribution. The solid curve, taken from Simien & de Vaucouleurs (1986), is a fit to the bulge-to-total ratios of normal galaxies derived from surface photometry and is the relation we used to obtain M_{bul} from M_{tot} and T. Not only do the overall gradients of the kinematic and photometric Δm_{bul} relations agree well, but there is even some evidence that the kinematic data points follow the photometrically derived curve better than the simple linear fit. Furthermore, although we have forced the agreement of Δm_{bul} at $T = -5$, note that the two Seyfert ellipticals nicely bracket $\Delta m_{bul} = 0$, which suggests not only that the gradients but also the zero points of the B/D versus T relations for Seyferts and normals are the same.

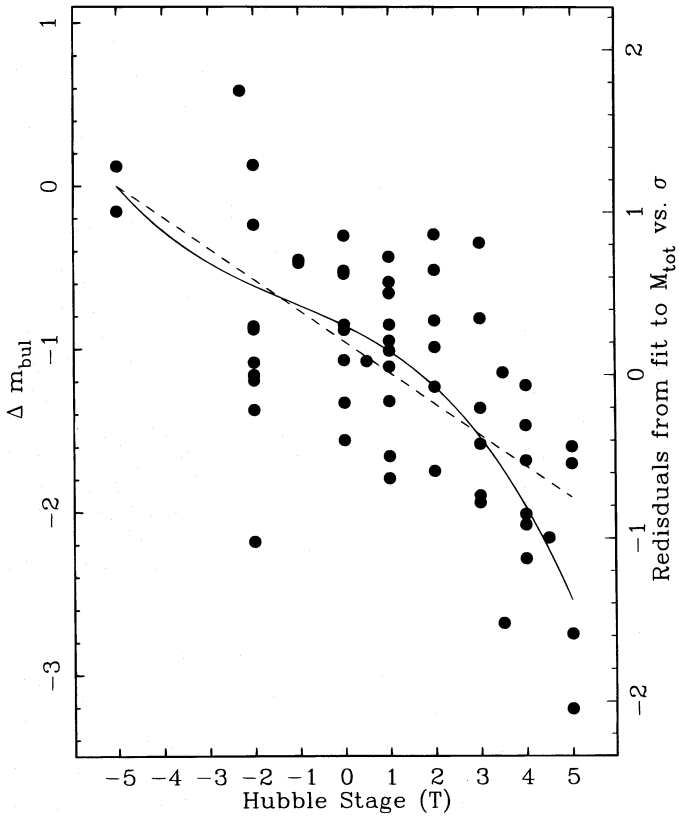

FIG. 2.—Residuals of the M_{tot} vs. σ_* relation (Fig. 1*b*) are plotted vs. Hubble type. The right-hand Y-axis gives the value of ΔM_{tot}. A linear fit is shown as the dotted line. The left-hand Y-axis gives the inferred bulge correction adopting the value of $\Delta m_{bul} = 0$ at $T = -5$. The solid line is taken from Simien & de Vaucouleurs (1986) and gives Δm_{bul} derived from surface photometry. Note that the kinematically and photometrically derived bulge-to-total ratios agree remarkably well.

This remarkable agreement between the photometric and kinematic determinations of Δm_{bul} suggests that the bulge-to-disk ratios in Seyfert galaxies have the same Hubble type dependence as normal spirals. It would, of course, be interesting to confirm this result using surface photometry of Seyferts to separate bulge and disk light explicitly. However, we suspect that photometric bulge-disk separation for the Seyferts may not produce substantially different results. This is partly because the errors on the individual B/D ratios are large and technique dependent (see Simien & de Vaucouleurs 1986) and partly because the errors on σ_* already dominate the scatter on the Faber-Jackson relation. Finally, we note that the agreement of the Hubble type dependences for Seyferts and normal spirals and the correspondence of these with the mean bulge-to-total ratios of spirals support our use of Δm_{bul} in estimating M_{bul}, as does the tightness of the σ_*-M_{bul} relation.

3.2. *Comparison of $L \propto \sigma_*^n$ for Seyfert and Normal Galaxies*

Although most studies of the Faber-Jackson relation have focused on developing a distance indicator for elliptical galaxies, it is also an important tool for studying the physical properties of spheroidal stellar systems. It is important, therefore, to compare our results for Seyferts with those of other classes of galaxies. We first consider the Faber-Jackson relation for normal galaxies.

Previous studies have shown that spiral bulges and ellipticals generally follow the same $L \propto \sigma_*^n$ relation. Deviations

have been claimed using rather small samples for a number of subclasses of galaxies, including barred galaxies, edge-on galaxies (Kormendy & Illingworth 1983), S0 galaxies (Dressler 1987), and powerful radio galaxies with morphological peculiarities or strong emission lines (Smith, Heckman, & Illingworth 1990). Some authors have also commented on a possibly shallower slope for low-luminosity systems (see, e.g., Tonry 1981).

In view of these uncertain results, Whittle (1992c) re-examined the $L \propto \sigma_*^n$ relation for a large sample of normal spirals and ellipticals using photometric and stellar kinematic data compiled from the literature. Corrections for Galactic and internal absorption, disk light, and redshift were applied in the same manner as for the Seyferts. Direct bulge-disk separation from surface photometry was available for galaxies in the Simien & de Vaucouleurs (1986) sample, which allowed a test for systematic deviations resulting from the use of mean bulge-disk ratios. A breakdown of the correlation and regression results is given in Table 1 of W92c. Spiral bulges and ellipticals were found to follow the same $L \propto \sigma_*^n$ relation with a gradient $n \sim 3$–4, although the spirals show more scatter. There is no apparent distinction in the relationships for highly inclined or barred galaxies. The best fit for galaxies with explicitly determined bulge-to-disk ratios is indistinguishable from that using mean ratios estimated from the Hubble type.

In comparing the Faber-Jackson relations for Seyfert and normal galaxies, we are interested in three aspects of the relation: the gradient, the zero point, and the degree of scatter. In Figure 1*a*, the dashed line shows the fit to normal spiral and elliptical galaxies as displayed in Figure 4 of W92c. The gradient of this fit corresponds to $n = 3.15 \pm 0.15$ and has $\mathrm{FWHM}_*(-20) = 359 \pm 6$ km s^{-1}. The gradient for the Seyferts ($n = 2.7 \pm 0.3$) is slightly shallower than for normals, but this difference is probably not significant. Thus, the way in which velocity dispersion increases with luminosity in Seyferts points, at least in part, to an underlying dynamical similarity between the bulges of Seyferts and the bulges of normal galaxies.

What is more striking, however, is the difference in zero point. Figure 1*a* shows that the $L \propto \sigma_*^n$ relation for Seyferts is shifted to lower velocity dispersion relative to the relation for normal galaxies. The difference amounts to -0.10 in $\log \sigma_*$ at $M_{\mathrm{bul}} = -20.0$ or, alternatively, -0.62 mag in M_{bul} at $\sigma_* = 150$ km s^{-1}. Thus, we may view Seyferts as having either velocity dispersions $\sim$20% lower or bulges $\sim$80% brighter than normal galaxies. Figure 3 shows histograms of $\Delta\sigma_* = \sigma_{\mathrm{gal}} - \sigma_{\mathrm{FJ}}$ for Seyfert galaxies, normal spirals ($0 \leq T \leq 6$), and ellipticals. As expected from Figure 1, the Seyfert residuals show a negative offset, with mean $\Delta \log \sigma_*$ different from that of normal spirals at a significance level of 0.002%. The Seyfert residuals also show a narrower distribution than normal spirals at a significance level of 0.4%. Interestingly, the Seyfert residuals fall completely within the envelope of the spirals. As we discuss below, this raises the possibility that Seyferts simply avoid galaxies with large positive $\Delta \log \sigma_*$, rather than actually cause a shift to negative $\Delta \log \sigma_*$. When comparing $\Delta \log \sigma_*$ for Seyferts and ellipticals, the difference in the means has the same statistical significance; however, the two distributions have statistically indistinguishable variances.

We feel the offset of the Seyferts in the Faber-Jackson plot is real. As discussed in Paper I, we have checked our velocity dispersion measurements against both simulated data and other published measurements and find no systematic offset toward lower values (see Paper I, Figs. 5, 6, and 7). We also trust our estimates of M_{bul} since, as discussed above, we find evidence that supports our use of the normal galaxy bulge/disk ratios in deriving M_{bul} from M_{tot}.

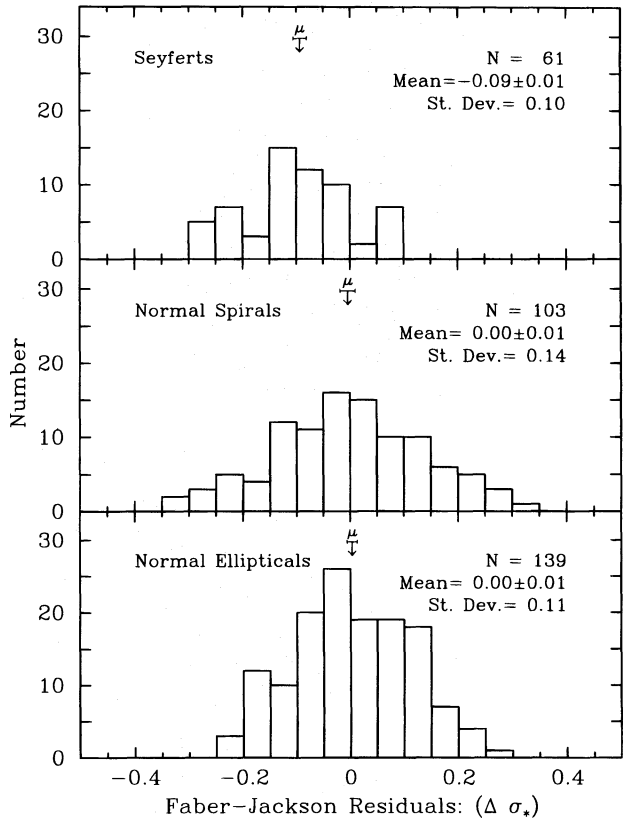

FIG. 3.—Distribution of residuals ($\Delta\sigma_*$) from the normal Faber-Jackson relation (Fig. 1*a*, *dashed line*) are shown for Seyferts spirals and ellipticals. Note the offset for Seyferts and the broad distribution for spiral galaxies.

We consider several possible explanations for this offset: the influence of a black hole, an unusual central surface brightness, and an unusual mass-to-light ratio. If Seyferts contain supermassive black holes, one might expect that the near-nuclear stellar dynamics would be altered. However, the offset is in the opposite sense to that expected since the gravitational influence of a black hole should lead to larger, not smaller velocity dispersions. Our results do not, however, argue against the presence of a black hole since our nuclear apertures are usually too large to be sensitive to stellar kinematics on scales of a few tens of parsecs.

Another possibility is that although Seyfert bulges are offset on the Faber-Jackson plot, they nevertheless lie on the fundamental plane for spheroidal systems. Since the fundamental plane is defined by σ_*, M_{bul}, and $\langle\mu\rangle$, the mean surface brightness, we would require Seyfert bulges to have fainter surface brightnesses by $\sim$1 mag per square arcsec compared to normal bulges. At present we consider such a significant difference to be unlikely since Seyferts are typically galaxies with prominent bulges, though it is clearly important to obtain accurate surface photometry to check this possibility.

A more plausible explanation for the Faber-Jackson offset is a difference in mass-to-light ratios. The direction of the offset suggests that Seyferts have lower mean M/L ratios than normal galaxies, i.e., they are more luminous for a

given mass. Since the nuclear nonstellar contribution has been removed (and was in any case not significant), a difference in M/L must then stem from a difference in stellar population. The most obvious possibility is that Seyferts have younger near-nuclear populations. This conclusion is also consistent with the notion that Seyferts have had more numerous and more severe encounters with neighboring galaxies in their pasts which has resulted in higher star formation rates.

Our conclusion of lower M/L ratios in Seyferts is consistent with a wide range of other studies, using the Faber-Jackson relation, the Tully-Fisher relation, and other signatures of strong star formation. For example, Smith et al. (1990) found that powerful radio galaxies with peculiar morphologies and/or strong emission lines have bluer colors and a similar offset from the standard elliptical $L \propto \sigma_*^n$ relation (see Fig. 17). They suggest that these galaxies have experienced recent mergers, possibly with spirals, providing more rotational support, lower velocity dispersion, and lower M/L ratio. In § 6 we further compare the properties of Seyfert and radio galaxies. Using optical rotation curves, Afanasiev (1981) found values of M/L 1–3 times lower than normal for a sample of 17 Seyferts. In a related analysis of the Tully-Fisher relation for a larger sample of Seyferts, Whittle (1992c) also found offsets suggesting lower values for M/L.

Studies that focus on other diagnostics of star formation have recently been reviewed by Heckman (1991), Whittle (1992c), and Heckman et al. (1995). Briefly, evidence for significant nuclear and near-nuclear star formation comes from mid- and far-infrared luminosities and colors (see, e.g., Rodríguez-Espinosa, Rudy, & Jones 1987; Heckman et al. 1989; Maiolino et al. 1994), near- and mid-infrared absorption features (Terlevich et al. 1990; Oliva et al. 1995), integrated *IUE* spectra (Heckman et al. 1995), and optical multiaperture photometry (Zasov & Lyuti 1973, 1981; Afanasiev, Pimonov, & Terebizh 1982; Zasov & Dibai 1970; Zasov & Niezvestny 1989). Taken together, there is considerable evidence that Seyferts may have experienced significant recent star formation, leading to lower M/L ratios and offsets on the Faber-Jackson and Tully-Fisher planes.

There is, however, a potential complication in this picture. We noted earlier (Fig. 3) that the scatter on the Faber-Jackson relation for Seyferts was significantly less than for normal spirals. Yet if we are to interpret the Faber-Jackson offset as a result of lower M/L ratios, we would also expect increased, not decreased, scatter, since the enhanced star formation would vary from galaxy to galaxy. It seems odd that Seyferts would all have the same change in the stellar population relative to normals.

A possible resolution of this is hinted at in Figure 3, which shows the distributions of the Faber-Jackson residuals. Although the distribution of residuals for Seyferts is narrow and offset in the mean, it falls within the distribution of residuals for the normal spirals. Thus, we may view the Seyferts not as a shifted population, but as avoiding galaxies with positive Faber-Jackson residuals. If the Faber-Jackson residuals are in fact due to variation in M/L, then we conclude that Seyfert activity avoids galaxies with high M/L, i.e., old populations with no recent star formation. This explanation would also be consistent with the apparent infrequency with which Seyfert activity is found in normal elliptical hosts. An obvious physical interpretation is that systems of high M/L have very little nuclear gas with which to fuel or initiate nuclear activity. With this interpretation, we see normal spirals as having a range of M/L corresponding to a range of star formation histories. From these normal spirals, only those with high star formation histories can go on to develop Seyfert activity.

To summarize, we have examined the correlations of $M_{\rm tot}$ and $M_{\rm bul}$ with σ_*. The relation between σ_* and $M_{\rm tot}$ allows a kinematic derivation of bulge-to-disk ratio for Seyferts as a function of Hubble type. This relation agrees with both kinematic and photometric derivations of bulge-to-disk ratio in normal spirals. This suggests that Seyferts have normal bulge-to-disk ratios and supports our use of $\Delta m_{\rm bul}$ in deriving $M_{\rm bul}$ from $M_{\rm tot}$. The gradient of the $L \propto \sigma_*^n$ relation for Seyfert galaxy bulges is normal, suggesting an underlying dynamical similarity between the bulges of Seyferts and the bulges of normal galaxies. However, we find that the zero point of the $L \propto \sigma_*^n$ relation for Seyferts is offset to lower σ_* relative to normal spirals. If Seyferts lie on the fundamental plane, then the Faber-Jackson offset implies a rather low central surface brightness, which we feel to be unlikely. Instead, we suggest the offset results from lower M/L ratios in Seyferts, consistent with a number of other studies that show significant star formation in Seyferts. Since normal spirals can also have low M/L, an alternative perspective is that Seyferts simply avoid galaxies with high M/L, with corresponding old populations and little or no interstellar material.

3.3. *Galaxy Rotation and Velocity Dispersion*

Another way to examine the structure of galaxies is to compare the nuclear stellar velocity dispersion, σ_*, with the (deprojected) rotation velocity of the disk, $V_{\rm max}$. Since the former measures the potential of the bulge, while the latter measures the potential of the disk and/or halo, a comparison of these two velocities reflects the relationship between bulge, disk, and halo. Simple theory informs us how these two velocities should be related. For a mass density profile $\rho \propto r^{-\alpha}$, solutions to the collisionless Boltzmann equation give $V_{\rm max} = (\alpha)^{1/2}\sigma_*$ (Gott 1977). While flat rotation curves imply $\alpha \sim 2$, steep bulge profiles imply $\alpha \sim 3$, suggesting $V_{\rm max}/\sigma_*$ should lie in the range $2^{1/2}$–$3^{1/2}$. A number of studies of normal spirals find that this is in fact the case, with some tendency for $V_{\rm max}/\sigma_*$ to increase for later type spirals with smaller bulges (Whitmore & Kirshner 1981; Fall 1987; Whittle 1992b; and Franx 1993). We next perform a similar analysis for Seyfert galaxies and ask whether they follow the same trends as normal galaxies.

In Figure 4*a* we plot the full galaxy rotation amplitude corrected for inclination, $\Delta V_{\rm rot}^c$ $(=2 \times V_{\rm max})$, versus the nuclear velocity dispersion, σ_*. Excluding elliptical galaxies ($T < -2$) and galaxies with inclinations less than 25°, we find a weak correlation with $R = 0.39$ and $P(\text{null}) = 3.4\%$. The best linear fit (OLS bisector [*solid line*]) has approximately unit slope and is offset from $y = x$ (*dashed line*) by 0.17 in $\log \Delta V_{\rm rot}^c$. This offset corresponds to a mean value for $V_{\rm max}/\sigma_*$ of 1.7, which is consistent with the value found for normal galaxies.

The S0 galaxy NGC 5252, marked by the cross, is known to have counterrotating gas and stars on scales $\sim 10''$ (Held, Capaciolli, & Capellaro 1992 also confirmed in our long-slit data). The $\Delta V_{\rm rot}$ compiled in W92a was taken from larger radii where gas and stars corotate but with lower $V_{\rm max}$ than the inner counterrotating region. We have therefore excluded this object from the analysis.

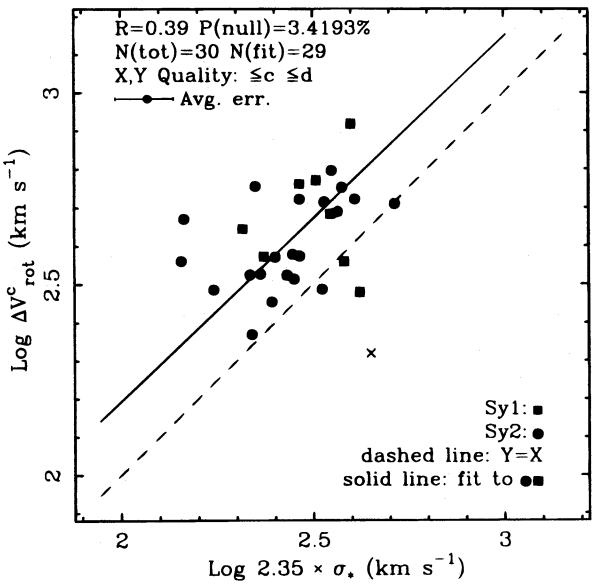

FIG. 4a

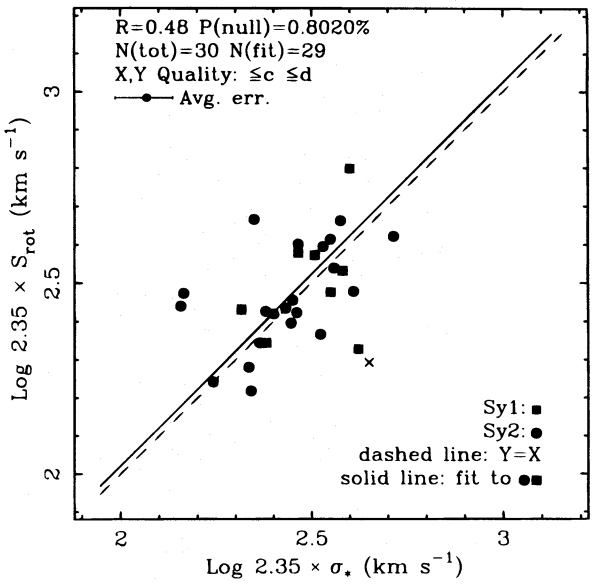

FIG. 4b

FIG. 4.—(*a*) Full galaxy rotation amplitude corrected for inclination, ΔV^c_{rot}, is plotted against σ_*. The solid line is a fit to the data using the OLS bisector, while the dashed line traces $X = Y$. The separation between the two lines corresponds to $V_{max}/\sigma_* \simeq 3^{1/2}$. The point flagged with a cross is NGC 5252. We exclude this object since it has counterrotating gas and stars. (*b*) New parameter S_{rot}, which is the velocity dispersion expected from the relation of σ_* and ΔV^c_{rot} for normal galaxies corrected for Hubble type (see eq. [2]), is plotted against σ_*. The rough agreement between σ_* and S_{rot} suggests no systematic differences in the stellar kinematics of Seyfert and normal galaxies.

Partial correlation analysis shows a dependence on Hubble type similar to that seen in previous studies of normal galaxies, with $R_{V_{max},\sigma} = 0.39$ increasing to $R_{V_{max},\sigma|T} = 0.44$. We can correct for this Hubble type dependence by using the relation for normal galaxies given in W92b to define a new parameter, S_{rot}:

$$\log S_{rot} \equiv \log V_{max} - 0.16 - 0.31 \times T \, . \qquad (2)$$

This equation simply estimates the value of σ_* expected from ΔV^c_{rot} using the mean relation between V_{max}/σ_* and T determined empirically from normal spirals.

In Figure 4*b* we plot S_{rot} versus σ_* for the same galaxies shown in Figure 4*a*. The correlation strength has improved, with $R = 0.48$ and $P(\text{null}) = 0.8\%$, and the best linear fit suggests $S_{rot} \approx \sigma_*$. Within the quality of the data, therefore, the relation between ΔV^c_{rot} and σ_* for Seyferts is identical to the relation for normal spirals. We conclude that the bulge-disk (and possibly halo) structure of Seyferts, defined in kinematic terms, is normal.

It is interesting to compare the results of the two virial relations we have just explored, since they rely on different measures of the gravitational field. The Faber-Jackson relation combines a photometric measure, M_{bul}, with a kinematic one, σ_*, and reveals an offset between Seyfert galaxies and normal galaxies. In contrast, the S_{rot} versus σ_* relation combines two kinematic measurements and finds no offset between Seyfert and normal galaxies. This supports our suggestion that it is the photometric parameter, M_{bul}, and not the kinematic parameter, σ_*, that underlies the offset on the Faber-Jackson relation, and this in turn supports our conclusion that Seyferts have lower mean mass-to-light ratios than normal spirals. If, for example, the Faber-Jackson offset was instead caused by an unusual bulge stellar velocity field, such as enhanced rotational support, we would have expected a similar offset in the S_{rot} versus σ_* plot.

Although there are no systematic differences for Seyferts in the S_{rot} versus σ_* plot, there is more scatter than in the same plot for normal galaxies. Specifically, we find that face-on galaxies ($i < 35°$) are more scattered than the edge-on galaxies. Inclination estimates and thus inclination corrections to rotational velocities are significantly more sensitive to errors in the axial ratios at low inclinations. This effect may be responsible for the increased scatter for face-on galaxies in this diagram. However, the same analysis applied to the sample of normal galaxies shows no increase in scatter for face-on galaxies. Although this may simply reflect a greater uncertainty in the Seyfert inclinations, another possibility is a higher incidence of warped disks in Seyferts, and these would undermine inclination estimates, particularly at low inclination. A high incidence of warps in Seyferts would be interesting since they may be associated with recent tidal perturbations and/or the presence of nonaxisymmetric potentials necessary for nuclear fueling.

We conclude from this section that the kinematic links between bulge, disk, and possibly halo are the same in Seyferts as in normal spirals, at least in the mean. This supports the notion that the nuclear stellar velocity dispersion, as measured by σ_*, is essentially normal for the Seyfert bulges and that the Faber-Jackson offset is indeed the result of a lower mean mass-to-light ratio in the Seyferts.

4. KINEMATICS OF GAS AND STARS

4.1. *The Gravitational Component of the Gas Kinematics*

We next compare the velocity field of stars and ionized gas using the stellar velocity dispersion, σ_*, and the width of the [O III] λ5007 emission line. Since σ_* measures the basic gravitational velocity in the near-nuclear regions, a comparison with the [O III] line width should show the degree to which the velocity field of the NLR gas has a gravitational origin. This addresses one of the fundamental ques-

tions of AGNs: does the gas velocity field reflect active nuclear processes or motion in the nuclear potential? Previous work suggests that both are relevant. Using M_{bul} and ΔV^c_{rot} as virial parameters, Whittle (1992b, c) finds good correlations with [O III] FWHM supporting a dominant gravitational component but with somewhat broader emission lines for objects with strong bipolar radio sources, which indicates a jet-driven velocity component. Since M_{bul} and ΔV^c_{rot} are only indirect gravitational parameters, it is important to repeat this analysis with σ_*, which we regard as a more direct and therefore robust measure of the nuclear gravitational field.

In the earlier analysis using M_{bul} and ΔV^c_{rot}, only the [O III] FWHM parameter was used to measure gas velocity. Since we now have direct measurements of both star and gas velocities through the same aperture, we may attempt a slightly fuller comparison. In particular, since the [O III] profiles are rarely Gaussian, we can consider several different parameters that correspond, loosely, to the width of the profile core, trunk, base, and wings, respectively: FWHM, FW20, IPV20, and IPV10 (the IPV parameters are derived by excluding 20% and 10% of the area from the blue and red wings of the profile and are defined more fully in Whittle 1985a). Ideally, we would have similar parameters for the stellar velocity "profile," but limited signal-to-noise ratio and our method of analysis allow only a Gaussian characterization with its single width parameter, σ_*.

We consider first the FWHM parameters. Figure 5 shows [O III] FWHM plotted against $FWHM_*$ for all 66 Seyfert galaxies with qualities $Q(\sigma_*) \leq$ c and $Q(FWHM_{[O\ III]}) \leq$ c. The dashed line shows $Y = X$, while the solid line shows the OLS bisector fitted to all the data. Although we have a much larger sample, Figure 5 is similar to the earlier plots of Wilson & Heckman (1985) and Terlevich et al. (1990). There is a moderately strong correlation with considerable scatter ($R_P = 0.48$, $Z_K = 3.7$, P(null) = 0.005%) and best-fit gradient somewhat flatter than unity. Figure 7*a* shows the distribution of residuals, ΔW(FWHM), about the line $Y = X$, where $\Delta W(FWHM) = \log FWHM([O\ III]) - \log FWHM_*$. The distribution has zero mean and standard deviation 0.20. Overall, therefore, the emission- and absorption-line FWHM values correlate and are numerically similar. This strongly supports the view that gravitational dynamics plays a key role in the NLR.

Interestingly, excluding the worst quality data ("c") does not improve the correlation statistics. Furthermore, the formal errors on individual objects are often less than the scatter about the fit. Clearly, much of the scatter is real, and other processes besides gravity influence the emission line kinematics. In particular, there are a few galaxies that stand away from the rest of the sample with exceptionally broad [O III] lines, and these force the best-fit gradient to be flatter than unity. As we discuss below, these objects have strong linear radio sources, and it seems fairly certain that at least some of the NLR gas is being accelerated by bipolar jets. We discuss more fully in § 4.2 the origin of scatter in Figure 5.

We now consider the rest of the [O III] profile, using FW20, IPV20, and IPV10 to replace FWHM in the previous analysis. A similar correlation strength is found using FW20 [$R = 0.49$, $Z_K = 3.9$, P(null) = 0.002%], while somewhat weaker correlations are found for the IPV parameters [e.g., $R = 0.40$, $Z_K = 3.1$, P(null) = 0.11% for IPV20]. As an example, Figure 6 shows a plot of IPV20 versus $FWHM_*$, where the solid line gives the OLS bisector best fit and the dashed line gives $IPV20_{[O\ III]} = IPV20_*$, assuming a Gaussian stellar profile with IPV20 = 1.0884 × FWHM. As before, we define residuals from the equality (*dashed*) line, and Figure 7*b* shows the distribution of these for IPV20, with mean 0.15 and standard deviation 0.18. The distribution of residuals for FW20 and IPV10 also have positive mean. Overall, therefore, it seems that the [O III] profile base and wings are not as closely tied to the stellar velocity dispersion as the [O III] profile core and also exhibit higher velocities than simple gravitational motion. Similar results have been found in studies using M_{bul} in place of σ_* by Veilleux (1991b) and Whittle (1992c).

It is not clear how to interpret these results physically.

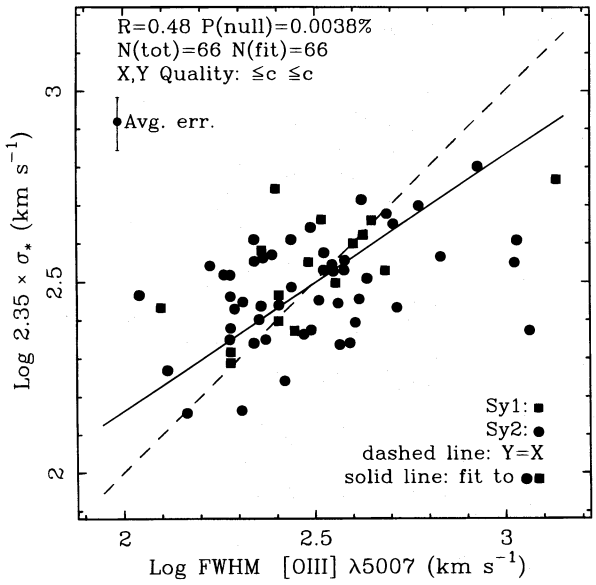

FIG. 5.—$FWHM_{[O\ III]}$ vs. $FWHM_*$ is shown. The solid line is a fit using the OLS bisector method (see § 2), and the dashed line shows $X = Y$. Objects with qualities $Q(\sigma) \leq$ c and $Q(FWHM_{[O\ III]}) \leq$ c are plotted.

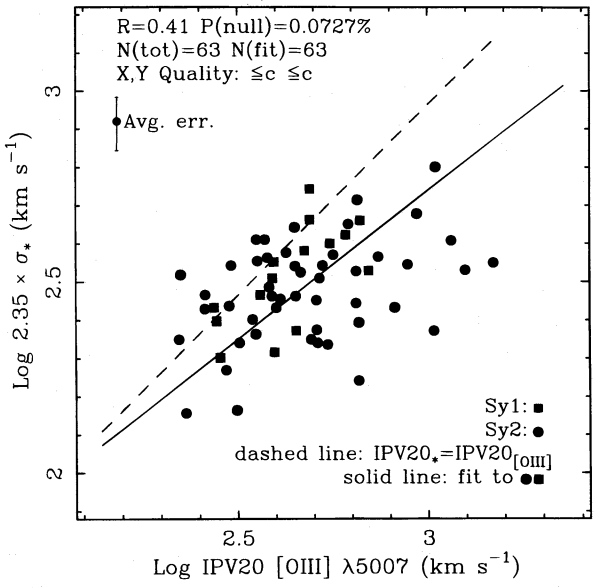

FIG. 6.—$IPV20_{[O\ III]}$ vs. $FWHM_*$ is plotted. The dashed line shows equal emission and absorption line IPV20 assuming a Gaussian stellar velocity distribution. Objects with qualities $Q(\sigma) \leq$ c and $Q(IPV20_{[O\ III]}) \leq$ c are plotted.

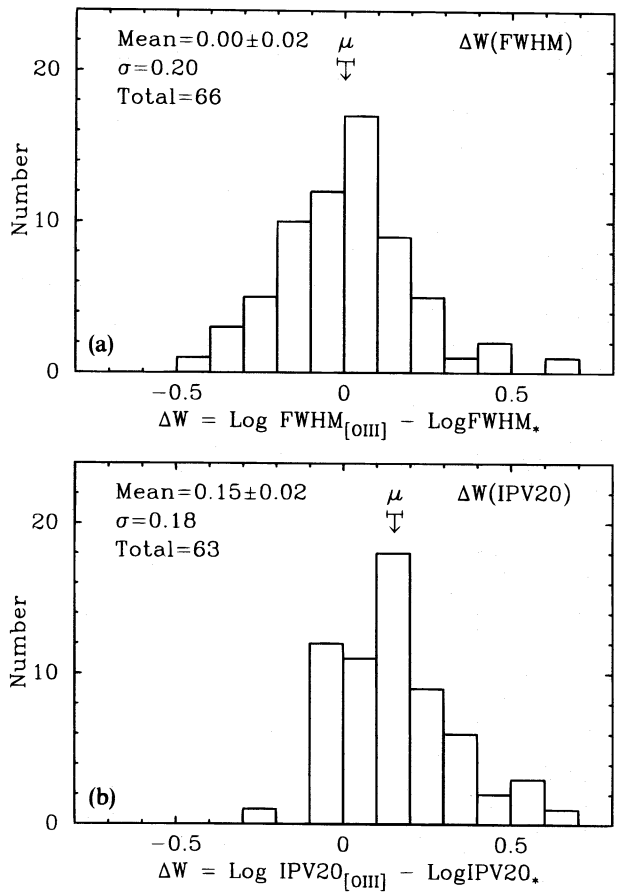

FIG. 7.—Histograms of ΔW(FWHM) and ΔW(IPV20). The shift in the lower histogram reflects the strong wings relative to a Gaussian profile characteristic of [O III] emission lines.

The main limitation to our understanding comes from our inability to characterize the stellar velocity "profile" as anything other than a Gaussian. Since [O III] profiles are almost always more peaked than Gaussian, then approximate equality of stellar and [O III] core widths guarantees that lower in the profile, the [O III] width will be greater than the stellar width. A more explicit comparison must await a fuller, non-Gaussian, determination of the stellar velocity profile. Although this type of analysis has recently been developed, it requires very high quality data, and even then it is notoriously difficult to detect weak broad wings. Unfortunately, even a full comparison of [O III] and stellar "profiles" may not reveal their interdependence, since each depends on both velocity field and luminosity distribution. Because the [O III] emission depends on nuclear illumination, it may be much more centrally concentrated than the starlight. Thus, even if the [O III]–emitting gas moved with the stars at all radii, [O III] profiles may show broader wings than stellar "profiles," even when both are taken through the same aperture.

A more straightforward interpretation of our results is, of course, that the gas contributing to the [O III] wings is highly nuclear and its velocity field is dominated by non-gravitational forces. Thus, the wing width parameters become less correlated with the gravitational parameters and indicate larger velocities. Also, the fact that the [O III] wings are often asymmetric lends some support to this interpretation, since profile asymmetry implies a radial flow that could be related to the nuclear acceleration mechanism. Although this seems most plausible, the alternative scenario of fully gravitational motion with infall may also be consistent with our results (see Whittle 1992d)

We note finally that the objects with extremely broad [O III] FWHM are not as well separated from the main group on the plots using the base and wing width parameters. This is probably because a number of these objects have relatively stubby profiles in which the core has been broadened by the radio jet driven bipolar flow (Whittle 1985b; Veilleux 1991a, b).

To summarize, we have compared the kinematics of gas and stars in the nuclear regions of Seyfert galaxies using the widths of the [O III] λ5007 emission line and the nuclear stellar velocity dispersion. We find a moderately strong correlation with $\mathrm{FWHM}_{[\mathrm{O\,III}]} \simeq \mathrm{FWHM}_*$. This confirms earlier results using indirect gravitational parameters, and suggests the NLR gas kinematics is defined largely by motion in the bulge gravitational field. However, there is considerable real scatter showing that secondary factors are also relevant. Repeating the analysis using parameters that measure the width of the [O III] profile in the base and wings shows weaker correlations and gas velocities greater than gravitational. Unfortunately, interpreting these differences is not straightforward. Possibilities include non-gravitational acceleration for the highest velocity gas or fully gravitational motion in a steep potential in which the line emission is more compact than the starlight.

4.2. *Secondary Influences on NLR Kinematics*

As noted above, the scatter on Figure 5 is probably not all observational. First, the scatter is approximately independent of our data quality ratings a, b, and c. Second, our average 1 σ error on σ_* is only 0.07 in the log (see error bar plotted in Fig. 5), which is significantly less than the 1 σ scatter about the best-fit line and the $Y = X$ line of 0.15 and 0.20, respectively. Finally, our estimate for a typical error on [O III] FWHM for quality a or b is only $\sim$0.04 in the log, corresponding to an rms difference between different measurements of $\sim$10% (see Paper I). Once again, this is significantly less than the observed scatter in Figure 5.

We conclude that at least some of the scatter in Figure 5 is real. Since the underlying correlation reflects the similar gravitational motion of gas and stars, we infer that additional processes must also influence the kinematics of ionized gas. In this section we try to identify some of these additional processes by examining the dependence of the scatter in Figure 5 on a number of other properties, such as radio characteristics, galaxy morphology, inclination, and Seyfert type.

4.2.1. *Radio Emission*

There is already considerable evidence for a close link between ionized gas velocities and radio emission. First, there is a correlation between [O III] FWHM and radio luminosity (see, e.g., Wilson & Willis 1980). Second, spectroscopy of Seyferts with double or triple radio morphology shows high-velocity components coincident with the radio lobes (see, e.g., Whittle et al. 1988). Third, on plots of [O III] FWHM against the indirect gravitational parameters M_{bul} and $\Delta V^c_{\mathrm{rot}}$, Seyferts with relatively strong linear radio sources lie offset from the main sample, with higher [O III] line widths (see, e.g., W92a, b). All these results point to an

interaction between radio plasma and ionized gas that results in gas acceleration.

Is similar evidence found in our own sample, using σ_* as a gravitational monitor? In Figure 8, we replot Figure 5 (i.e., $FWHM_{[O\ III]}$ vs. $FWHM_*$), this time flagging objects with linear radio morphology. Linear sources with log $L_{1415} > 22.5$ are marked as plus signs, while less luminous sources are marked as open circles (L_{1415} is the radio luminosity at 1415 MHz in W Hz^{-1}). First, if we exclude the linear radio sources, we obtain a best-fit line very close to the line $Y = X$, confirming the equivalence of star and gas velocities for normal (nonradio) Seyferts. Second, of the five objects with much broader [O III] lines (NGC 1068, NGC 1275, Mrk 3, Mrk 78, and Mrk 622), four have known luminous linear radio sources. The radio morphology of the fifth object (Mrk 622, marked as a cross) is not known, but its broad stubby [O III] profile and much narrower Hβ profile together suggest that it too has a linear radio source. It seems, therefore, that for at least these extreme objects, the radio source accelerates the ionized gas well beyond typical gravitational velocities.

However, apart from these extreme objects, we find that the remaining luminous linear radio sources are not well separated from the rest of the sample. Application of Student's t-test to the distributions of ΔW(FWHM) for the two groups gives a 67% probability of having the same means. This is puzzling since Whittle (1992b, c) found much clearer offsets using ΔV^c_{rot} and M_{bul} in place of σ_*. Most of this difference, however, stems from our smaller sample size and the particular objects in question. For example, we could not obtain reliable velocity dispersions for MCG 8-11-11, Mrk 6, and Mrk 463, all of which have powerful linear radio sources and are offset from the gravitational correlations in plots using M_{bul} and ΔV^c_{rot}. Our sample also has a disproportionate number of linear sources that lie close to the fit using any of the three virial parameters (e.g., Mrk 533, NGC 2110, NGC 2992, and NGC 7319). Repeating Whittle's analysis for our sample using M_{bul} and ΔV^c_{rot} shows no significant separation for the subset of linear sources with more moderate line widths. Conversely, we find that objects that lie off the correlations using M_{bul} and ΔV^c_{rot} also lie off the correlation using σ_*. An interesting discrepancy is NGC 4151, which has a rather large (though somewhat uncertain) value of σ_* for its M_{bul} and ΔV^c_{rot}, reducing its offset from the gravitational relation in Figure 8. Overall, we conclude that the apparent differences between our results and those in W92b, c are less pronounced than it at first seems and that luminous linear radio sources do generally have supervirial line widths, though clearly not all do.

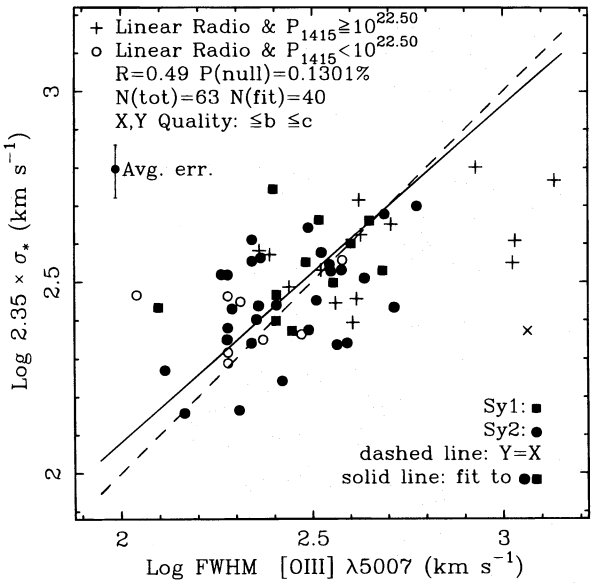

FIG. 8.—$FWHM_{[O\ III]}$ vs. $FWHM_*$ with linear radio sources with $L_{1415} > 10^{22.5}$ marked as plus signs and those with less luminous linear sources marked as open circles. The more luminous linear sources tend to have positive residuals to the fit suggesting interaction between the radio source and NLR gas. Note the change in the slope of the fit to the remaining objects as compared to Fig. 5.

It is interesting to compare our results with those of similar studies of powerful radio galaxies by Smith et al. (1990) and of compact steep spectrum (CSS) radio galaxies by Gelderman (1994). Smith et al. find emission-line velocities comparable to stellar velocities, despite the presence of very luminous linear radio sources. An example is 3C 120, which is in our sample and has the narrowest [O III] lines of all the luminous linear radio sources. For the Smith et al. sample, however, the radio sources are generally much larger than the host galaxies, and the jets that feed them apparently escape without significantly disturbing the kinematics of the nuclear gas. In contrast, Gelderman finds that CSS radio galaxies tend to have rather broad [O III] lines (although a comparison with gravitational velocities has not yet been made). Although these objects have very luminous radio sources, they are similar to the Seyferts in the sense that their radio sources are contained within the host galaxy. It would seem, therefore, that even if radio sources are luminous and jetlike, they also need to be approximately cospatial with the ionized gas for a strong kinematic interaction to occur.

In conclusion, our results broadly support those of previous studies that indicate that Seyfert galaxies with luminous linear radio sources tend to have [O III] FWHM values that are broader than the gravitational widths because of interaction with the radio source. However, our analysis with σ_* is less clear-cut than with M_{bul} or ΔV^c_{rot}, which reminds us that the jet interactions are certainly not ubiquitous.

4.2.2. *Interacting and Disturbed Galaxies*

Recent studies using numerical simulations have shown that the distribution and kinematics of near-nuclear gas can be altered during galaxy interactions (see, e.g., Barnes & Hernquist 1991). In this section we investigate the possible dependence of [O III] line width on galaxy interactions and/or morphological peculiarities. To characterize the degree of interaction or disturbance, we use the parameter PC, perturbation class, as defined in W92a. PC is the maximum of the parameters DC and IAC, which rate the morphological disturbance and the nearness of a neighboring galaxy respectively on a scale of 1 (for least disturbed) to 6 (for most disturbed). These parameters are based on definitions given by Dahari (1985).

In Figure 9 we again plot $FWHM_{[O\ III]}$ versus $FWHM_*$, but now we flag barred galaxies and perturbed galaxies with PC > 4. We exclude the five objects with the most extreme [O III] widths since, as we discussed above, their gas kinematics are probably influenced by radio jets. With one exception, all of the high PC galaxies are offset from the fit to the unflagged points, shown as the solid line. The mean

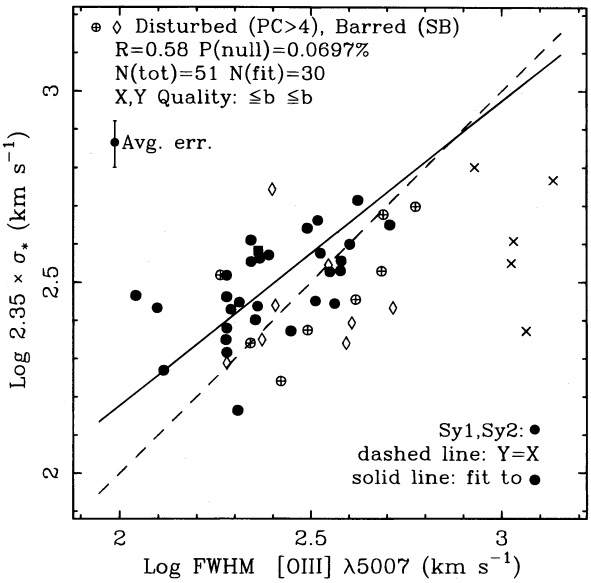

FIG. 9.—$FWHM_{[O\ III]}$ vs. $FWHM_*$ with barred and interacting galaxies flagged. Note the tendency for the interacting and morphologically disturbed galaxies (PC > 4) to have relatively large [O III] width. Barred galaxies appear more scattered than the remaining objects. Note the increase in R_P for the remaining objects.

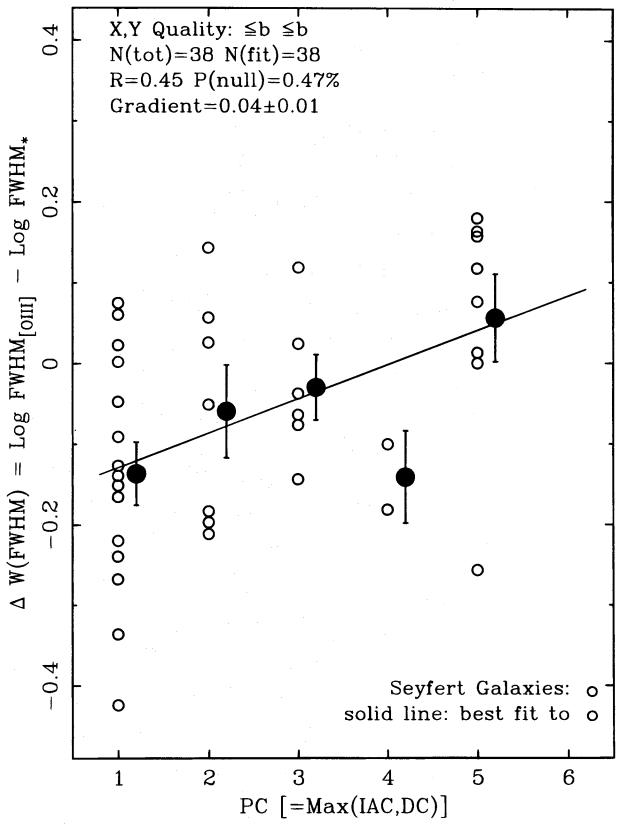

FIG. 10.—PC vs. ΔW(FWHM) is shown. The open circles represent individual objects, while the filled circles and error bars indicate the mean and standard deviation for each level of PC and are offset slightly for clarity. Note the trend for interacting and morphologically disturbed objects (i.e., those with high values of PC) to have relatively broader emission lines.

value of ΔW(FWHM) for the high PC subset is greater than the mean value for the remaining objects at a significance level of P(null) = 2%.

We can explore these results further by plotting ΔW(FWHM) versus PC. In Figure 10 the open symbols are the individual objects, while the solid points show the mean for each value of PC and its 1 σ error. There is a clear trend for the least disturbed objects to have relatively narrow emission lines, while the most disturbed objects have relatively broad emission lines. The solid line shows a fit to the open symbols [$R_P = 0.44$, $Z_K = 2.9$, P(null) = 0.6%]. This supports the earlier analysis using M_{bul} instead of σ_* (see W92c, Fig. 9). In that case, a plot of velocity offset against PC also shows that disturbed galaxies have relatively broader [O III] lines, with best-fit gradient almost identical to that found in Figure 10.

We note that some ambiguity exists in these results since a number of objects display more than one phenomenon that may be associated with kinematic disturbances in the NLR. For example, the object with the broadest emission lines in the sample is NGC 1275. It is not clear whether its extreme line width results from interaction of the radio plasma with the interstellar medium or from processes related to its disturbed morphology. Including this object as a highly interacting system (PC = 5) improves the correlation statistics in Figure 10 significantly.

These results suggest that perturbations to the galactic potential induced by a strong interaction provide a secondary influence on the gas kinematics in the NLR. We also note that objects that are reasonably isolated and undisturbed tend to have negative ΔW(FWHM), essentially subvirial emission-line widths. We discuss this tendency further in § 4.3.

4.2.3. *Barred Seyferts*

We have also flagged barred galaxies in Figure 9. Comparing with the remaining Seyferts (SA and SAB) shows only a marginal difference in position in the diagram. There is a slight tendency for the barred galaxies to have broader emission lines for their stellar velocity dispersions than the rest of the sample [P(null) = 12%], and a more significant possibility of a larger variance [P(null) = 6%]. This latter result is reflected in the fact that excluding the barred galaxies improves the correlation coefficient rather sharply, from $R_P = 0.43$ to $R_P = 0.60$. These results are consistent with Whittle's (1992c) finding that barred Seyferts had a larger scatter around the emission-line Faber-Jackson relation than the rest of the sample (correlation coefficients of 0.35 compared with 0.74). In the present analysis, because of the small number of objects and the overlap of interacting and barred galaxies, it is not clear whether it is the bar that affects the [O III] line width. However, since we reproduce the results of W92c, we tentatively associate barred galaxies with a portion of the scatter in the [O III] width versus σ_* diagram.

4.2.4. *Inclination*

We have also investigated the role of galaxy inclination in order to explore the form of the gas velocity field. Using ΔV^c_{rot} as gravitational parameter, Whittle (1992b) used several kinds of analysis to investigate the inclination dependence of the [O III] line width, finding that the NLR velocity field was neither fully in the galaxy plane nor fully independent of it. We can revisit these methods of analysis using σ_* as the gravitational parameter. For example, we performed a partial correlation analysis to see if the scatter in the [O III] FWHM versus σ_* plot is correlated with

projection factor, sin i. Since we found no correlation, we were unable to identify any systematic component of the NLR velocity field that is confined to the plane of the galaxy. In a related analysis, we plot in Figure 11 the line width ratio $\Delta W(\mathrm{FWHM}) = \log \mathrm{FWHM}_{[\mathrm{O\ III}]}/\mathrm{FWHM}_*$ against sin i, excluding morphologically disturbed objects (PC > 4), barred galaxies, and luminous linear radio sources. If the [O III] line widths were produced by rotation in the galaxy disk (case A [*dotted line*]), we would expect a correlation with sin i that began at $V_{\max}/\sigma_* = 3^{1/2}$ at $i = 90°$ and sloped down to 0 at $i = 0°$ (see § 3.3). If the NLR velocity field were purely random (case B [*dashed line*]), there should be no dependence on sin i, and star and gas velocities should be equal. From Figure 11 one can see that the data do not conform to either idealized velocity field but instead show considerable scatter with a slightly negative mean. From these data it seems we cannot make a general statement about the planar or nonplanar nature of the NLR velocity field. We note in passing that the equivalent analysis using $\Delta V^c_{\mathrm{rot}}$ does show a correlation, with the best-fit line falling between the two idealized cases, suggesting at least some disklike component to the NLR velocity field (W92b, Fig. 9).

4.2.5. *Seyfert Type*

One of the most basic attributes of an active galaxy is whether or not it has a visible broadline region. Does the presence of this region somehow influence the kinematics of the gas in the NLR? Note that a simple comparison of line width distributions for Seyfert 1's and Seyfert 2's gives misleading results since it depends on the particular samples chosen. Since bulge gravitational potential is a primary variable, we must compare the [O III] line widths of Seyfert 1's and 2's at the same bulge potential. In Figure 5 we plot with different symbols Seyfert 1–1.5 galaxies and Seyfert 1.8–2.0 galaxies. There is no discernible difference in their location on the plot. In a related analysis, we tried to identify the importance of the BLR using the flux ratio [O III]/Hβ (including both broad and narrow Hβ components) as third variable in a partial correlation analysis. No change in correlation strength was found. It seems, therefore, that the relationship between [O III] line width and stellar velocity dispersion is independent of apparent strength of the broad-line region. This is consistent with earlier results using the indirect gravitational parameters M_{bul} and $\Delta V^c_{\mathrm{rot}}$ (W92b, c), as well as the fact that [O III] line widths in low-redshift quasars, are similar to those of Seyferts.

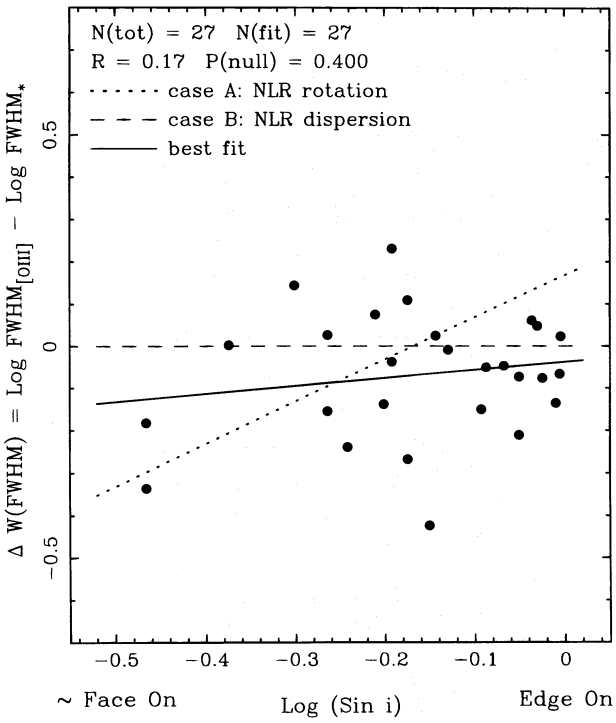

FIG. 11.—ΔW(FWHM) is plotted vs. log sin i. The dotted line shows the expected results for a purely rotational NLR, while the dashed line shows the case for dispersion. Although no distinction in the form of the velocity field is found for Seyferts as a class, individual objects could follow either of these cases.

The most obvious interpretation is that BLR gas and its associated activity does not interact directly with the NLR gas. A more subtle interpretation considers the distinction between type 1 and type 2 Seyferts to arise from viewing angle, as in "unified" schemes. In this case, the change from type 1 to type 2 follows a change in viewing an obscuring disk from face-on to edge-on. If the NLR is rotationally supported and coplanar with this obscuring disk, then we expect Seyfert 2's to have broader lines than Seyfert 1's at a given σ_*. The fact that they do not argues against this particular picture, and we conclude that the NLR velocity field is not confined to the plane of the inner obscuring disk.

It is interesting to combine this result with our related analyses of [O III] line width dependence on galaxy inclination (see § 4.2.4, above, and W92b). In this case we found that the NLR velocity field is not confined to the galaxy plane. Although it is possible that the NLR shares both outer and inner disk planes (which are not necessarily co-aligned) and is rotationally supported at all radii, it seems more likely that there is a velocity component perpendicular to these planes, which suggests at least some dispersion support.

4.2.6. *Redshift*

There are two possible biases in the relationship between gas and stellar velocity widths related to redshift that are important to investigate. First, our apertures sample a region the size of which depends on distance. Any systematic change in kinematic properties with radius may therefore show up as a change with redshift. Second, since the sample suffers Malmquist bias, at least at some level, any kinematic dependence on luminosity will also show up as a dependence on redshift. Two tests were performed on the full sample and on the various subsamples formed by excluding Seyferts with linear radio sources, bars, and disturbed morphologies, to identify any redshift dependence, each giving null results. First, the correlation statistics were unchanged for a low-redshift subsample with $cz < 4050$ km s^{-1} (close to the median redshift of the entire sample). Second, partial correlation analysis including redshift as third variable shows no change in correlation statistic. It seems, therefore, that our results are not sensitive to redshift and its associated biases.

4.2.7. *Differences between Emission-Line and Systemic Velocities*

Since we have found cases in which the emission-line widths are different from the stellar widths, it is interesting to ask whether the gas and systemic velocities are also different in these objects. This might arise in objects having net radial gas flow in which dust obscures a part of the velocity

field. To investigate this possibility, we have compared differences in gas and stellar velocities, presented in Table 4 of Paper I, with the scatter in the $FWHM_{[O\ III]}$ versus $FWHM_*$ diagram. Using both C80 and C_{med} for the gas velocity, we found no evidence for a link between differences in line centers and differences in line widths, either for the full sample or for various subsamples that exclude interacting galaxies, linear radio sources, and/or barred galaxies. A fuller examination of differences between gaseous and systemic velocities is planned for a subsequent paper.

4.3. *Subvirial Emission-Line Gas Kinematics*

Since we have investigated possible additional factors that broaden the [O III] lines, it is interesting to return to our discussion of the agreement between [O III] and stellar FWHM. Our initial analysis of the whole sample found a good match in the mean with $FWHM_{[O\ III]} \simeq FWHM_*$ (see Figs. 5 and 7). However, if we now exclude all objects with secondary factors that broaden the [O III] lines (e.g., those with powerful linear radio sources or those with strong morphological peculiarities), then the remaining sample has a mean [O III] FWHM less than the mean stellar FWHM. This was already evident in Figure 9, where the best-fit line falls to the left of the $Y = X$ line, and in Figure 10, where the trend to unperturbed (PC = 1) Seyferts clearly has negative mean ΔW(FWHM). In Figure 12 we give the distribution of ΔW(FWHM) for all Seyferts without secondary kinematic perturbations. The mean value of -0.1 ± 0.03 corresponds to $FWHM_{[O\ III]} \simeq 0.8\ FWHM_*$. It does seem, therefore, that in the absence of any additional acceleration mechanisms, the [O III] line widths measured at the FWHM point are "subvirial" in the sense that they are less than the equivalent stellar velocity.

These findings help confirm and clarify previous results using the indirect parameters M_{bul} and ΔV^c_{rot} (W92b, c). For example, a fit to the "emission-line" Faber-Jackson plot (M_{bul} vs. [O III] FWHM) showed a significant offset from the normal Faber-Jackson relation. By itself, it was not possible to distinguish between subvirial [O III] FWHM or low values of M/L for Seyfert bulges (W92c). It now seems that both occur—the true Faber-Jackson relation (M_{bul} vs. σ_*) confirms a low M/L for Seyfert bulges, while our plot of [O III] FWHM versus σ_* shows [O III] FWHM to be subvirial to an extent that depends on secondary factors such as galaxy disturbance. Interestingly, using ΔV^c_{rot} to estimate σ_* yields an intermediate result with $FWHM_{[O\ III]} \sim 0.9 \times FWHM_*$ (W92b). This occurs because the sample excludes badly disturbed galaxies on practical grounds and so gives an offset between zero and the full value for undisturbed (PC = 1) Seyferts. In fact, it was this modest offset in the ΔV^c_{rot} relation, combined with the PC dependence of the emission-line Faber-Jackson relation, that had already suggested that both subvirial [O III] FWHM and low M/L ratios were present (W92c).

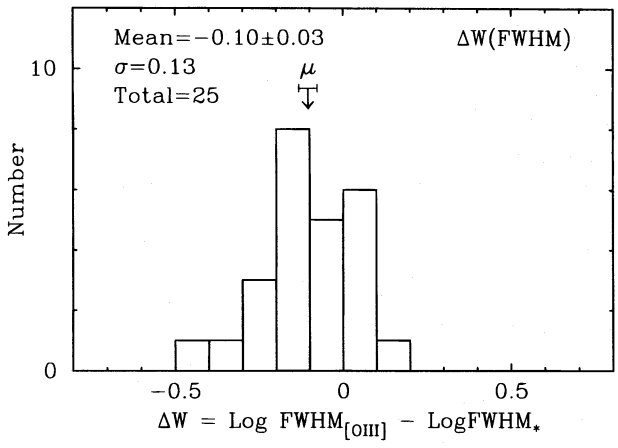

FIG. 12.—Distribution of ΔW(FWHM) after excluding objects suspected of having additional gas acceleration mechanisms is plotted. The negative mean value of ΔW(FWHM) suggests that the cores of Seyfert emission lines are subvirial.

How do we understand differences between [O III] and stellar FWHM and its dependence on galaxy disturbance? First, because the [O III] profiles are more peaky than Gaussians, a width parameter measured lower in the profile will show a better match to the stellar velocity, at least for the undisturbed galaxies. Indeed, a histogram of ΔW(FW20) (not shown) does show a distribution with a mean closer to zero. As discussed in § 4.1 above, this improvement in velocity match could result from an increasing gravitational velocity field at smaller radii, where the [O III] emission is progressively more intense relative to the starlight. Alternatively, it may simply reflect some other velocity-broadening mechanism that becomes important at smaller radii. Second, why is it that in the limit of no disturbance, the [O III] FWHM is only ~80% of the stellar FWHM? In fact, this seems to occur in normal galaxies (see, e.g., Phillips et al. 1986; Bertola et al. 1984; Fillmore, Boroson, & Dressler 1986). In this case, the ionized gas is thought to originate from stellar mass loss that settles through dissipation in a soft potential to inner regions in which the rotation curve has lower amplitude. If the NLR gas follows this pattern, then an integrated profile could well have FWHM less than $2.35 \times \sigma_*$. Finally, it seems that tidal perturbations are somehow associated with a better match between [O III] and stellar FWHM. This may reflect a stage in a sequence that starts with tidally triggered infall of gas to the nuclear regions, followed by dissipational settling in a soft potential. Thus, at early times when the perturbation is still evident, the gas has relatively high velocities associated with recent infall. As time passes, the perturbations diminish, and the NLR gas may relax through dissipation and come to equilibrium deeper in the potential where the rotation velocities are lower than the general stellar dispersion velocities.

5. STELLAR VELOCITY DISPERSION AND NLR LUMINOSITY

In addition to the relationship between bulge mass and NLR velocity field discussed above, other aspects of nuclear activity appear to be related to properties of the bulge. In particular, there is evidence that on kiloparsec scales, both optical emission-line luminosity and radio synchrotron luminosity are linked to the nuclear gravitational field. While previous studies made use of indirect virial parameters, we can now reexamine the connection between NLR luminosity and the host potential using our more direct parameter, σ_*. Because of the tight Faber-Jackson relation for Seyferts (see § 3.1), we expect that results using σ_* should be very similar to those found using M_{bul}.

5.1. *Emission-Line Luminosity*

It is well known that narrow-line luminosities correlate strongly with nuclear ionizing luminosity (see, e.g., Yee

1980; Shuder 1981)—a result that provides one of the main arguments that the gas is photoionized by the nuclear source. In addition to this correlation, however, the NLR luminosities may also be linked to bulge mass. For example, there is a moderately strong correlation between L_{5007} and M_{bul} (see Fig. 11*a* in W92c, R $\sim$ 0.54, best-fit $L_{5007} \propto L_{bul}^{2.5}$). We find a corresponding relation of similar strength between L_{5007} and σ_* shown in Figure 13 [$R_P = 0.58$, P(null) = 0.0003% gradient 4.6 $\pm$ 0.6 using OLS bisector].

As discussed in W92c, interpreting this correlation is not straightforward, since other factors that influence L_{5007} may themselves be related to σ_*. Several studies suggest that nuclear nonthermal luminosity depends on host galaxy luminosity (see, e.g., Dibai & Zasov 1985; Hutchings, Crampton, & Campbell 1984; Lawrence 1987; and see the review by Lawrence 1993). Also, L_{5007} is closely linked to L_{radio}, which itself may be linked to σ_* (see § 5.2 below). Moreover, the relation shown in Figure 13 reveals only an upper envelope, since nonactive galaxies with lower L_{5007} must fall below the relation. Nevertheless, other explanations invoking more direct association between L_{5007} and σ_* also deserve consideration. First, emission-line gas may originate as mass loss from bulge stars, and hence a more massive bulge may naturally provide a more substantial NLR. Second, a deeper potential well may produce higher pressures and therefore higher emissivities in the NLR gas. Finally, some additional heating of the NLR may be provided by shocks. Greater input might be expected in objects in which the virial speeds are higher, since the relative speeds between gas clouds will be higher and faster shocks will be produced.

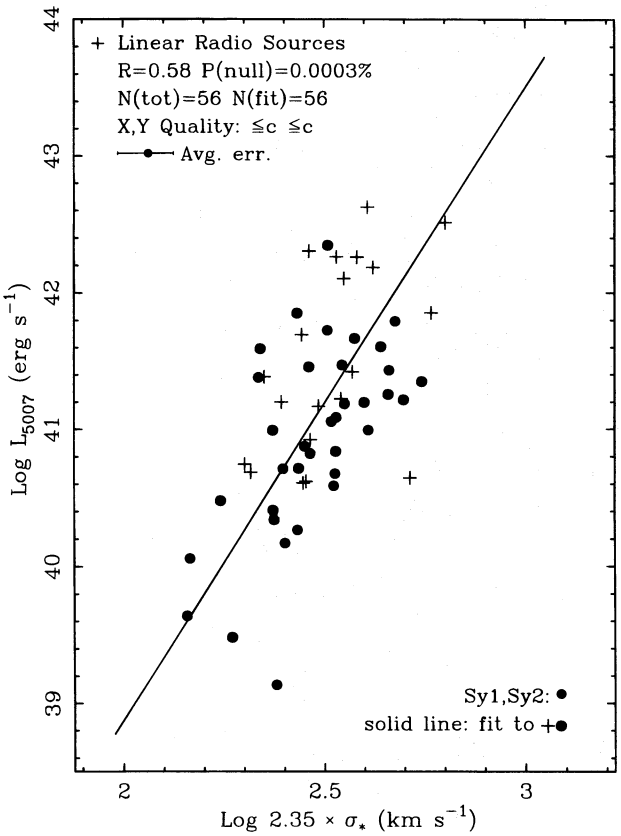

FIG. 13.—[O III] luminosity vs. σ_* is shown. We find a moderately strong correlation and a weak tendency for objects with linear radio sources to have relatively higher [O III] luminosity at a given σ_*.

We note in passing that the historically significant correlation between [O III] FWHM and L_{5007} (Phillips, Charles, & Baldwin 1983; Whittle 1985b) now seems to have an indirect origin. [O III] FWHM depends physically on σ_* (via gravitational acceleration) and L_{radio} (via jet acceleration), and the apparent correlation with L_{5007} stems simply from the dependence of L_{5007} on both L_{radio} and σ_* (see also W92c).

5.2. *Radio Luminosity*

The dependence of radio luminosity on host galaxy luminosity has been studied previously in a number of ways. For example, Sadler, Jenkins, & Kotanyi (1989) constructed the bivariate luminosity function, $\Phi(L_{radio}, L_{opt})$, for a complete sample of E and S0 galaxies and found that the fraction of galaxies containing luminous ($>10^{22}$ W Hz^{-1}) radio sources increases with increasing optical luminosity. They also show that a characteristic power, P_{30}, which marks the 70th percentile in radio luminosity, increases with bulge blue luminosity as $P_{30} \propto L_B^{2.2}$. More straightforward correlation studies have found similar results. For a sample of Markarian Seyfert 2 galaxies, Meurs & Wilson (1984) found a correlation between radio power and absolute optical magnitude. Also, Edelson (1987) found a relation of approximate form $L_{radio} \propto L_{gal}^2$ for the CfA sample of Seyfert galaxies. It seems, however, that bulge luminosity is the relevant parameter since these correlations are found to be significantly stronger when the disk light is removed (W92c, $R \sim 0.63$ with $L_{radio} \propto L_{bul}^{2.7}$).

Again, using σ_* in place of galaxy luminosity, we find a similar relation. Figure 14 shows a moderately strong correlation between σ_* and L_{1415} ($R_P = 0.55$, P(null) = 0.0014%, best-fit gradient 5.9 $\pm$ 0.7 with intercept 7.3 $\pm$ 1.7 using OLS bisector). A simple estimate using the Faber-Jackson gradient from § 3.1 yields $L_{radio} \propto L_{bul}^{2.2}$, consistent with previous results. We confirm, therefore, that the radio luminosity of Seyfert galaxies increases steeply with increasing nuclear potential. Interestingly, objects with linear radio sources (*plus signs*) appear to be more powerful at a given velocity dispersion by about 0.6 in the log or a factor of $\sim$4 [residuals from the fit differ at a significance level of P(null) = 0.8%, using Student's t-test].

What lies behind this relation between radio luminosity and bulge potential? We consider three possibilities. First, the energy input from the nuclear source itself may depend on bulge mass, perhaps through black hole mass and/or fueling rate. Although observational evidence for such a dependence is fragmentary, it seems at least plausible on theoretical grounds (see, e.g., Haehnelt & Rees 1993). Second, the size of the radio and line-emitting regions may also depend on the size of the bulge. This might arise naturally if an NLR can form only under certain conditions and if these conditions are found only within galactic spheroids, perhaps because of their associated ISM properties. Bigger bulges would then harbor bigger NLRs, which would have higher luminosity simply because of their larger volume. Finally, since emissivities depend on pressure, we might expect higher pressure environments to be more luminous. If the bulge ISM is hydrostatically supported, then those bulges with the deepest potentials and largest σ_* will have higher ISM pressures and therefore higher NLR luminosities, all other things being equal. This picture requires approximate pressure balance between the radio source, the NLR gas, and the other ISM components in the bulge.

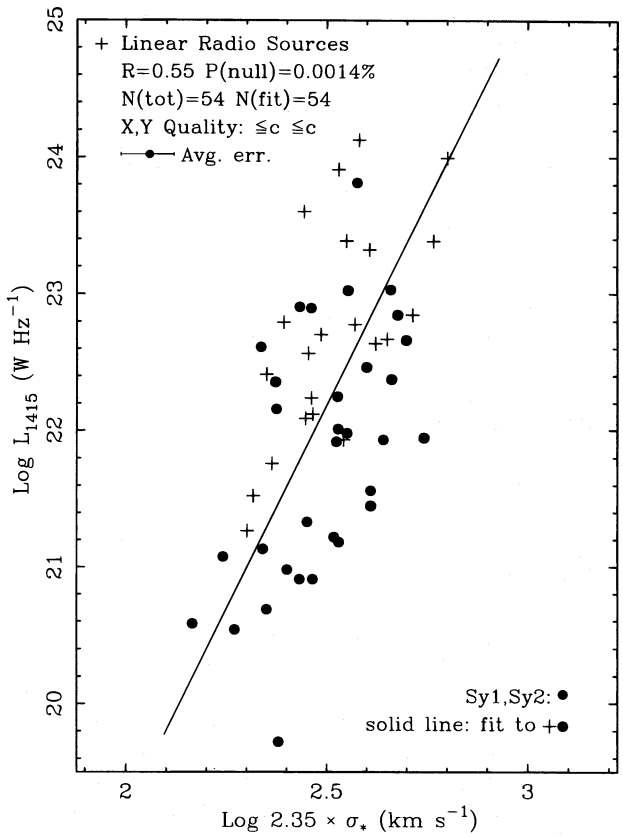

FIG. 14.—Radio luminosity at 1415 MHz is plotted against σ_*. We find a moderately strong correlation and a significant tendency for objects with linear radio sources to have relatively higher [O III] luminosity at a given σ_*.

Although this has not yet been shown to hold in detail, rough pressure estimates do support approximate pressure balance between the line-emitting and radio components (see, e.g., de Bruyn & Wilson 1978). In this context, we might understand the offset of the linear radio sources in Figure 14 (and to a lesser extent in Fig. 13) as resulting from higher pressures associated with the jet/ISM dynamical interaction.

To search for evidence of these processes, we have carefully compiled measurements of individual radio source properties from the literature. Using standard relations and assumptions (see, e.g., Miley 1980), we have used radio source size, flux, and spectral index to estimate radio source volumes and pressures. These parameters were used in a partial correlation analysis of the L_{1415} versus σ_* relation to examine the possibility that scatter in this relation depends on source volume or pressure. For sources with more than one radio component, we have considered both total and individual component measurements. We have also tried to use similar resolution data, favoring VLA A-array data if it exists. Most measurements were taken directly from the publications (see, e.g., Ulvestad & Wilson 1984a, b, 1989), although in some cases we made estimates from published radio contour maps.

Unfortunately, our analysis was unsuccessful in identifying a significant third parameter dependence in the L_{1415} versus σ_* relation, nor did we find a two-parameter correlation between σ_* and source pressure, either including or excluding the linear sources. We did, however, recover the two-parameter correlation between total radio source size and luminosity first noted by Ulvestad & Wilson (1984a; $R_P \sim 0.6$–0.8, depending on data quality and sample definition). Their preferred explanation is that more powerful jets burrow farther from the nucleus, although other possibilities are discussed.

While these null results are disappointing, especially our failure to identify a relation between radio source pressure and σ_*, we suspect that a number of factors have undermined our analysis. Most important is the limitation imposed by finite (and inhomogeneous) instrument resolution. For example, many sources are classified as "slightly resolved" ("S" in the scheme of Ulvestad & Wilson 1984a) and can give quite different results depending on the resolution of the study. Also, many of the smaller radio subcomponents are unresolved, yielding only upper limits to size or lower limits to pressure. The pressure estimates themselves, of course, incorporate a number of assumptions that may or may not hold true, especially in different contexts such as an aged dispersed radio source compared to a young jet-powered lobe component. We hesitate, therefore, to use these negative results to cast doubt on our general picture of an NLR whose luminosity depends on bulge potential because its size, pressure, and nuclear input may all depend on that potential.

Finally, we note here that the L_{1415} versus σ_* relation shown in Figure 14 sheds some light on the well-known correlation between radio luminosity and [O III] line width (see, e.g., Wilson & Willis 1980; Heckman et al. 1981; Whittle 1985b). Since [O III] line width depends principally on σ_* (see § 4 above), then at least part of the correlation between L_{1415} and [O III] line width must be of indirect origin, with L_{1415} standing in for σ_*. In fact, the L_{1415} versus [O III] line width correlation is significantly stronger than one would expect if it were only indirect. Since [O III] line width also depends on radio properties, through jet acceleration for the luminous linear sources, then part of the L_{1415} versus [O III] FWHM correlation is also of direct origin. Thus, radio luminosity is strongly tied to [O III] line width, with both direct and indirect links in place (see also W92c for a similar discussion arising from the L_{1415} vs. M_{bul} relation).

To summarize, we have found that the radio and emission-line luminosities in Seyfert galaxies are related to depth of the nuclear gravitational potential. This could result if more massive bulges harbor more luminous nuclear engines, have larger emitting regions, and/or have higher pressures and emissivities. Our attempt to clarify these possibilities using radio source sizes and pressures was unsuccessful, although difficulties in compiling a homogeneous and well-resolved sample probably played a role in weakening our analysis.

6. SEYFERT AND RADIO GALAXIES: CONTINUITY OF PROPERTIES

Although we have paid considerable attention to the radio properties of Seyfert galaxies, they are, of course, examples of radio-quiet AGNs, with relatively feeble radio sources compared to those found in radio galaxies. The origin of this division into radio-quiet and radio-loud sources is still poorly understood, with few clear observational inputs. The possible importance of host galaxy type is often cited; Seyfert galaxies are usually spirals, while radio galaxies are usually ellipticals, albeit peculiar ones (Smith et al. 1990). Since we have found a steep relation between

radio luminosity and bulge potential for Seyferts, we might expect AGNs with more massive host galaxies to have much higher radio luminosities. In this case, we can think of the division between radio-quiet and radio-loud objects not in terms of spiral and elliptical host galaxy types, but instead in terms of objects with low or high bulge mass.

We now look for continuity between the properties of radio-quiet AGNs (Seyferts) and radio-loud AGNs (radio galaxies), using host galaxy spheroidal mass (σ_* and M_{bul}) as our discriminating variable. We make use of the stellar velocity dispersions published by Smith et al. (1990) and the recent compilation of radio galaxy properties by Zirbel & Baum (1995). We also discriminate between FR I and FR II radio sources and between total and core radio power (L_{tot}, L_{core}). To allow comparison with our Seyfert data, we convert radio powers to 1415 MHz using the quoted spectral indices and V magnitudes to B assuming $B-V=1$ with no disk contribution. Unfortunately, it is not possible with this data set to isolate and remove those radio cores that are dominated by a compact flat spectrum component. For most of the sample, however, we suspect that the cores substantially reflect steeper spectrum emission from kiloparsec scales, which we consider to be the natural counterpart to the Seyfert radio sources.

First, we show the relations between σ_* and L_{tot} and between σ_* and L_{core} for the combined sample of Seyfert and radio galaxies (Figs. 15*a* and 15*b*, respectively; note that $L_{core}=L_{tot}$ for the Seyferts). In Figure 15*a* the solid line shows the best fit to just the Seyferts. Clearly, when considering total radio power, the radio galaxies fall well above the Seyfert relation. However, this is not true for the core power. From Figure 15*b* we see that the radio galaxy core powers fall right on the Seyfert relation and even overlap with the more luminous Seyferts [a t-test fails to distinguish between the Seyfert and radio galaxy residuals, with P(null) = 41%]. The best fit to the combined sample (Fig. 15*b* [*solid line*]) is essentially identical to the fit to the Seyferts alone. We note, however, that by themselves the radio galaxies do not show a correlation. Either no such relation exists or other sources of scatter, for example, a flat spectrum contribution and/or possible beaming effects, are dominant, even for kiloparsec-scale emission.

Interestingly, there may be evidence for an additional separation within the sample shown in Figure 15*b*. The Seyferts with linear radio sources and the cores of FR II radio galaxies are systematically more luminous than the Seyferts without the linear sources and the cores of FR I radio galaxies. Although there is some overlap in the distributions, it seems we can pair together the linear Seyferts with the FR II cores and the "nonlinear" Seyferts with the FR I cores. Figure 15*b* shows as the dashed and dotted lines the individual fits to the two groups, revealing approximately parallel relations offset by ~ 0.8 ($\sim \times 6$) in log radio power or ~ 0.12 in log σ_*. A t-test shows the two groups to have different residuals about either fit at the $\sim 0.004\%$ level. This intriguing distinction, if real, introduces yet

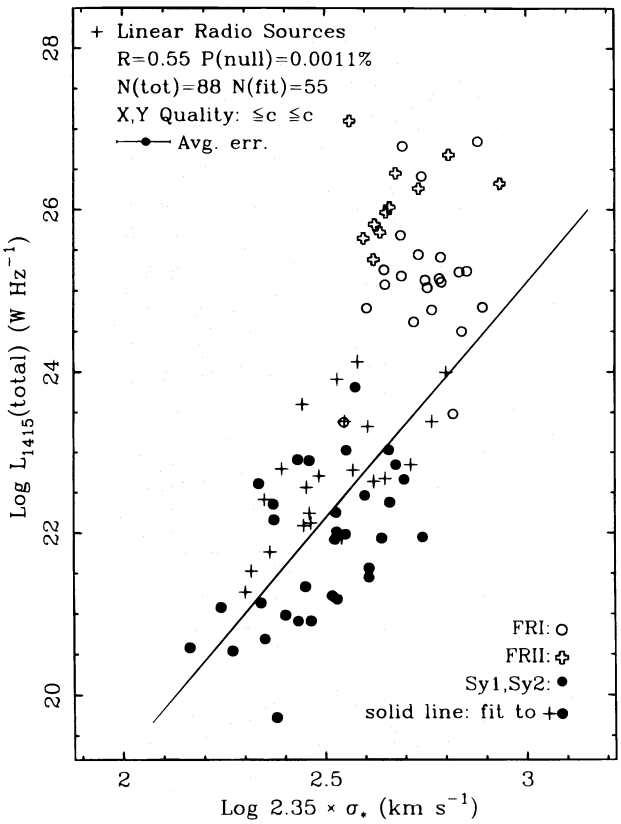

FIG. 15*a*

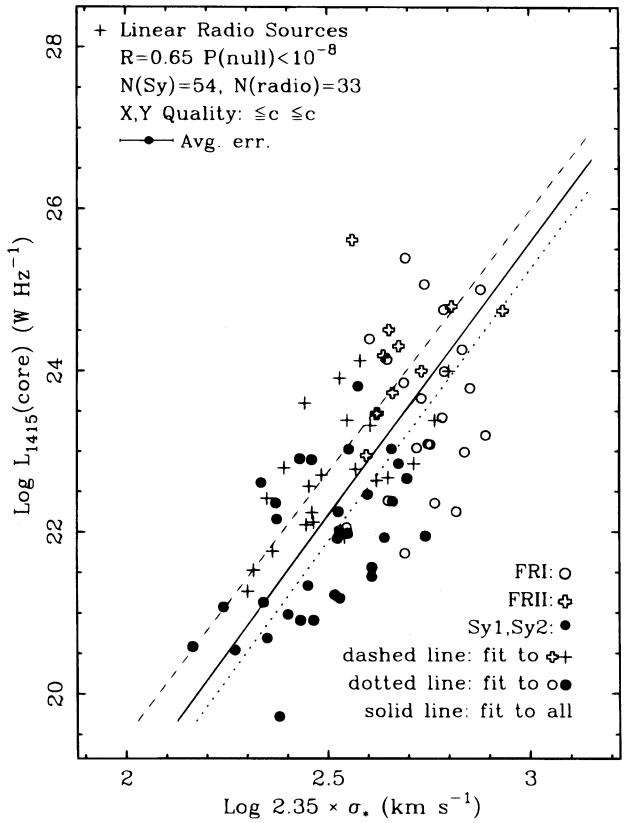

FIG. 15*b*

FIG. 15.—(*a*) Total radio luminosity at 1415 MHz vs. σ_* including FR I and FR II radio sources. The solid line is the fit to just the Seyferts. Note that the FR II sources tend to have lower velocity dispersions than FR I sources at a given radio luminosity. (*b*) Core radio luminosity at 1415 MHz vs. σ_* including FR I and FR II radio sources. The correlation statistics given in the upper left refer to all points plotted. The solid line is the fit to the combined sample and is not significantly different from the fit to the Seyferts alone (*solid line* in [*a*]). Note that the fit for FR II and Seyferts with linear sources (*dashed line*) lies above the fit to the FR I and remaining Seyferts (*dotted line*).

another aspect to the continuity between radio properties of Seyferts and radio galaxies, namely the possibility that the FR I/FR II dichotomy in radio galaxies can be traced down into the Seyfert luminosity range.

To some extent, these results are also found when we use M_{bul} in place of σ_*, as shown in Figures 16*a* and 16*b*. Here the sample size has increased dramatically because of the greater availability of galaxy magnitudes compared to σ_*. As before, when we consider total radio power, the radio galaxies lie well above the Seyfert relation, but when we consider only core radio power, the radio galaxies form a natural extension of the Seyfert population. In Figure 16*b* the combined sample shows a strong correlation ($R \sim 0.75$) spanning ~ 6 mag in M_{bul}, with approximate form $L_{rad} \propto L_{opt}^{3.2}$. In our sample, the radio galaxies alone do not show a strong correlation, although in a study of 3CR radio galaxies, Fabbiano et al. (1984) did find a correlation, and, as noted in W92c, an extrapolation of their relation passes right through the Seyfert sample. Clearly, when combined with the Seyferts, the correlation for the entire sample is quite compelling. Note that the presence of upper limits hardly affects our conclusion, and while a common dependence on redshift might artificially strengthen the relation it cannot be a major influence because the gradient is too steep. The possible separation into Seyferts with or without linear sources and FR I or FR II cores is somewhat less clear than in Figure 15*b*, although a *t*-test shows that the distribution of residuals about fits to either group are different at less than the 0.0001% level. The separation is also apparent in the 3CR sample of Fabbiano et al. (1984).

How do we interpret these results? In § 5.2 we discussed the relation between radio luminosity and bulge mass in the context of Seyferts alone, suggesting that more massive bulges may (1) harbor more massive black holes, (2) provide more fuel via mass loss from bulge stars, (3) have larger emitting regions, and (4) have higher ISM pressures, all of which may promote more radio emission. The results of this section suggest that these mechanisms may also apply to the radio sources in radio galaxies—at least to that part of the radio source that is located within the host galaxy. It may be possible to probe at least the hot, confining, ISM component of the bulge using its X-ray luminosity. In their study of X-ray, optical, and radio properties of early-type and radio galaxies, Fabbiano et al. (1984) and Fabbiano, Gioia, & Trinchieri (1989) indeed find evidence for a close link between this hot component and the radio source. First, simple density estimates suggest that the hot component can confine the weaker radio sources as well as the cores of the stronger sources. They also find that the radio luminosity from the weaker sources correlates with the X-ray luminosity of the hot ISM component, which suggests a close relation between the two. At higher luminosity the correlation is still present, but the origin of the X-rays is thought to be nuclear and active and to reflect a fueling rate that itself depends on the hot component through its cooling flow. Either way, the mass of the galaxy sets the

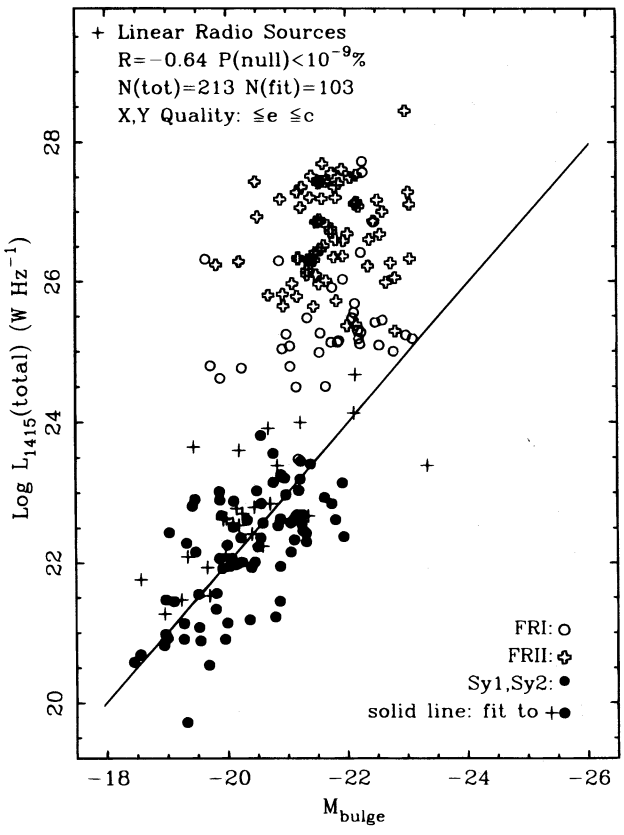

FIG. 16*a*

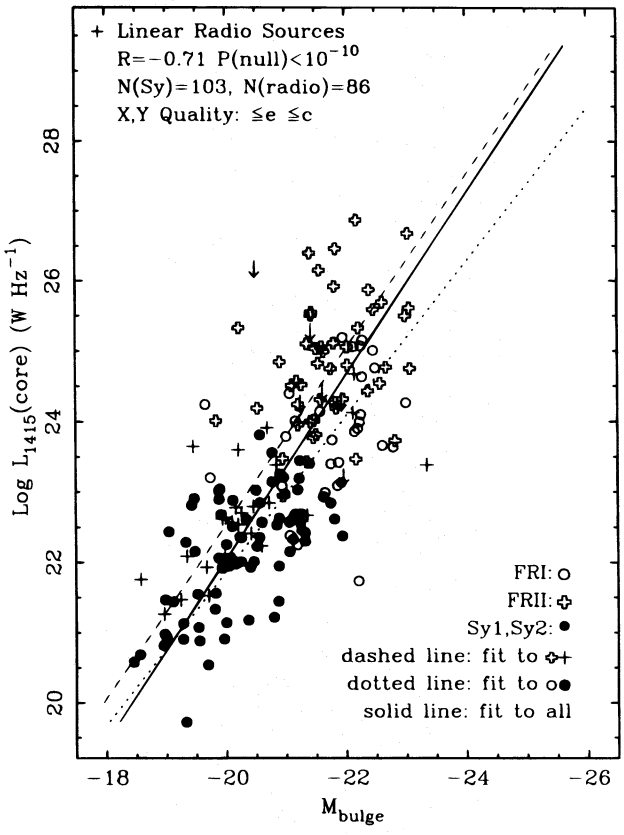

FIG. 16*b*

FIG. 16.—(*a*) Total radio luminosity at 1415 MHz vs. M_{bul} including FR I and FR II radio sources. The solid line is the fit to just the Seyferts. Note that the FR II sources tend to have lower velocity dispersions than FR I sources at a given radio luminosity. (*b*) Core radio luminosity at 1415 MHz vs. M_{bul} including FR I and FR II radio sources. The correlation statistics given in the upper left refer to all points plotted. The solid line is the fit to the combined sample and is not significantly different from the fit to the Seyferts alone (Fig. 15*a*, *solid line*). Note that the fit for FR II and Seyferts with linear sources (*dashed line*) lies above the fit to the FR I and remaining Seyferts (*dotted line*).

potential in which the hot component resides, and this in turn affects the origin and emergence of the radio source. In this picture, it makes sense that the total radio source powers do not correlate well with the galaxy mass, since the extended components are now influenced by the IGM the properties of which may bear little relation to the host galaxy. Indeed, the conditions required for radio source "breakout" from the galaxy are found to depend not only on the radio source power but also on the prominence of the hot ISM halo. Clearly this hot component plays an important role in influencing radio source development, and it in turn is influenced by the galaxy potential. Finally, we should not forget that these correlations represent upper envelopes, since many nonactive galaxies lie below the relation. The mechanisms discussed above become relevant only if a nuclear engine is being fueled and generating a radio source.

Understanding the possible division between subgroups of different radio morphology is more uncertain. At a given bulge mass (i.e., σ_* or $M_{\rm bul}$), it seems that the more "jetlike" sources have higher radio luminosity, i.e., the Seyferts with linear sources and the cores of FR II radio galaxies. Of course, the core morphology itself is not part of our study, but if a well-collimated high-power jet is seen on large scales, then presumably this same jet must pass through the core region. In this case, we consider the jet contribution as a second parameter, with bulge mass setting the basic context for the radio source origin and development, while jet prominence further enhances the source luminosity. The influence of the jet could take several forms: direct input through turbulent entrainment, providing dynamical pressures in excess of the hydrostatic pressure, pushing larger source sizes, or systematically greater Doppler boosting. An alternative way to look at this is to assume that less powerful jets are unable to form a linear structure (for Seyferts) or the FR II structure (for radio galaxies), probably because of their interaction with the gaseous halo which itself scales with the bulge mass.

Having found significant continuity between the radio properties of Seyferts and radio galaxies, we now return to the Faber-Jackson relation and ask whether the radio galaxies also resemble the Seyferts in this context. In particular, are they offset from the standard relation for normal bulges? Figure 17 shows the Faber-Jackson plot for Seyferts and radio galaxies, with data on the radio galaxies taken from Smith et al. (1990). Although the radio galaxies do not show a good correlation on their own, they form a natural extension to the Seyfert galaxy sample and, as a group, are clearly offset from the relation for normal galaxy bulges (*dashed line*). The fit to the combined sample (*solid line*) is essentially identical to the fit to the Seyferts alone. As we discussed in § 3.2, the Faber-Jackson offset is best explained as a low M/L ratio, and therefore younger population, relative to normal galaxies. Smith et al. did, of course, discuss this interpretation in some detail for their own sample. Here, however, we wish to stress the similarity and continuity with our Seyfert sample.

In summary, by focusing on galaxy bulges, we have found evidence for unity and continuity between radio-quiet and radio-loud AGNs. Seyferts and radio galaxies both fall on the same steep relation between galactic scale radio luminosity and bulge mass, highlighting the importance of the bulge in the fueling and/or development of all galactic scale radio sources—weak or powerful. Thus, we suspect the division into spiral or elliptical hosts arises from a more fundamental dependence of radio emission on bulge mass. Further similarities include the tendency for more jetlike sources to have more luminous radio sources at a given bulge mass and the offset placement on the Faber-Jackson plot. All these results promote the view of an AGN population whose galactic scale radio properties change continuously with bulge mass.

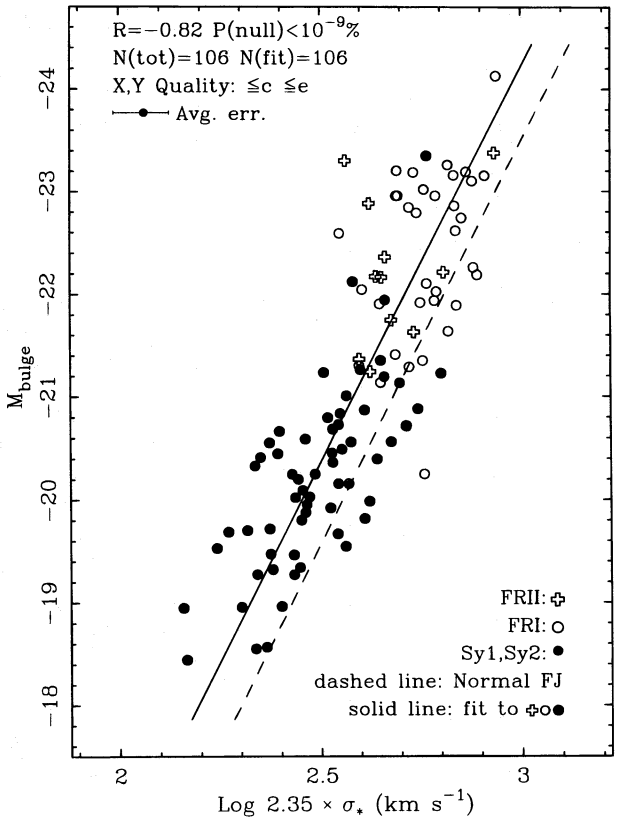

FIG. 17.—Faber-Jackson relation for Seyfert and radio galaxies from Smith et al. (1990) is plotted. The radio galaxies are also offset from the relation for normal galaxies. The solid line shows the fit to the combined sample using the OLS mean regression. As in Fig. 1*a*, the dashed line shows the $L \propto \sigma_*^n$ relation for normal galaxies.

7. CONCLUSION

In Paper I we presented measurements of the stellar velocity dispersion, σ_*, and [O III] profile width for a large sample of Seyfert galaxies. Here we have used these measurements to study the importance of the central gravitational field in Seyfert galaxies.

The Seyferts define a tight correlation between σ_* and the bulge absolute magnitude, $M_{\rm bul}$, which is estimated from the total magnitude and a Hubble type–dependent disk correction. The correlation closely matches the Faber-Jackson relation for normal spiral bulges, which suggests that Seyfert bulges are basically normal in their kinematic makeup. The Seyfert relation is, however, offset to higher bulge luminosities. Our preferred interpretation of this offset is that Seyferts have lower mean mass-to-light ratios. Either Seyferts have experienced higher than average star formation or they avoid systems with older stellar populations. This is consistent with the notion that Seyferts experience more interactions than normal spirals. We also analyze diagrams plotting σ_* against both $M_{\rm tot}$ and $\Delta V_{\rm rot}^c$,

and we find evidence for a normal kinematic relation between bulges and disks in Seyferts.

We have examined the relationship between σ_* and [O III] profile width, and we have found that the NLR velocity field is determined, in large part, by the bulge potential. The correlations are weaker with [O III] base and wing width parameters, although the interpretation of this is not yet clear.

There is considerable real scatter in these line width correlations, which shows that other factors are also relevant. In particular, objects with kiloparsec-scale linear radio sources can have significantly broader [O III] lines, which confirms that interaction with an expanding radio source can accelerate the NLR gas. We also find that Seyferts which are tidally distorted have broader [O III] lines. In the absence of these additional factors, the "unperturbed" [O III] FWHM are $\sim$80% of the stellar FWHM, which suggests that the gas may have settled through dissipation to a region where the local rotation velocities are lower than the global stellar dispersion velocity. We find that the kinematic relations do not depend on galaxy inclination or Seyfert class, which suggests that the NLR gas is confined neither to the plane of the galaxy nor to the plane of an inner obscuring disk.

Correlations have also been found linking the radio and emission-line luminosities with the depth of the gravitational potential. These relationships suggest that Seyferts with larger bulges also have more powerful NLRs. More massive bulges may have more powerful central engines, higher fueling rates from stellar mass loss, larger emitting regions, and/or higher pressures and emissivities. We attempted, without success, to distinguish empirically between some of these possibilities.

We found that the relation between radio power and spheroidal mass also applies to the cores of radio galaxies. This highlights the continuity between properties of radio-quiet and radio-loud AGNs and suggests that the commonly assumed division into spirals and ellipticals may in fact result from a more fundamental dependence of radio source properties on bulge mass. We also find some evidence for more "jetlike" sources to be more luminous at a given bulge mass, for both Seyferts and radio galaxies. We also note that the radio galaxies, like the Seyferts, are offset from the normal galaxy Faber-Jackson relation. All these results point to the fundamental similarity of the Seyferts and radio galaxies and to the importance of the bulge in determining the properties of the galactic scale radio source.

We would like to thank Mercedes Richards, Andrew Wilson, Martin Ward, Richard Gelderman, Richard Patterson, Bob O'Connell, Alan Bridle, Esther Zirbel, Steffi Baum, and Sylvain Veilleux, the referee, for helpful discussions and for their efforts to improve this paper.

REFERENCES

Afanasiev, V. L. 1981, AZh Pis'ma, 7, 390
Afanasiev, V. L., Pimonov, A. A., & Terebizh, V. Y. 1982, AZh Pis'ma, 8, 579
Barnes, J. E., & Hernquist, L. E. 1991, ApJ, 370, L65
Bender, R., Burstein, D., & Faber, S. F. 1992, ApJ, 399, 462
Bertola, F., Bettoni, D., Rusconi, L., & Sedmak, G. 1984, AJ, 89, 356
Busko, I. C., & Steiner, J. E. 1989, MNRAS, 238, 1479
Dahari, O. 1985, ApJS, 57, 643
de Bruyn, A. G., & Wilson, A. S. 1978 A&A, 64, 433
Dibai, E. A., & Zasov, A. V. 1985, Soviet Astron., 29, 273
Djorgovski, S., & Davis, M. 1987, ApJ, 313, 59
Dressler, A. 1987, ApJ, 317, 1
Dressler, A., Lynden-Bell, D., Burstein, D., Davies, R. L., Faber, S. M., Terlevich, R. A., & Wegner, G. 1987, ApJ 313, 42
Edelson, R. A. 1987, ApJ, 313, 651
Fabbiano, G., Gioia, I. M., & Trinchieri, G. 1989, ApJ 347, 127
Fabbiano, G., Miller, L., Trinchieri, G., Longair, M., & Elvis, M. 1984, ApJ, 277, 115
Fall, S. M. 1987, in Nearly Normal Galaxies from the Planck Time to the Present, ed. S. M. Faber (New York: Springer), 326
Fillmore, J. A., Boroson, T. A., & Dressler, A. 1986, ApJ, 302, 208
Franx, M. 1993, in IAU Symp. 153, Galactic Bulges, ed. H. DeJonghe & H. Habing (Dordrecht: Reidel), 243
Gelderman, R. 1994, Ph.D. thesis, Univ. of Virginia
Gott, J. R., III. 1977, ARA&A, 15, 235
Haehnelt, M. G., & Rees, M. J. 1993, MNRAS, 263, 168
Heckman, T. M. 1991, in Massive Stars in Starburst Galaxies, ed. C. Leitherer, T. Heckman, C. Norman, & N. Walborn (Cambridge: Cambridge Univ. Press), 289
Heckman, T., et al. 1995 ApJ, 452, 544
Heckman, T. M., Blitz, L., Wilson, A. S., Armus, L., & Miley, G. K. 1989, ApJ, 247, 403
Heckman, T. M., Miley, G. K., van Breugel, W. J. M., & Butcher, H. R. 1981, ApJ 247, 403
Held, E. V., Capaciolli, M., & Capellaro, E. 1992, in AIP Conf. Proc. 254, Testing the AGN Paradigm, ed. S. S. Holt, S. G. Neff, & C. M. Urry (New York: AIP), 613
Hutchings, J. B., Crampton, D., & Campbell, B. 1984, ApJ, 280, 41
Isobe, T., Feigelson, E. D., Akritas, M. G., & Babu, G. J. 1990, ApJ, 364, 104
Kormendy, J., & Illingworth, G. 1983, ApJ, 265, 632
Lawrence, A. 1987 PASP, 99, 309
———. 1993, in The Nearest Active Galaxies, ed. J. Beckman, L. Colina, & H. Netzer (Madrid: Consejo Superior de Investigaciones Cientificas), 3
Maiolino, R., Ruiz, M., Rieke, G. H., & Keller, L. D. 1995, ApJ, 446,561
Meurs, E. J. A., & Wilson, A. S. 1984, A&A, 136, 206
Miley, G. 1980, AR&A, 18, 165
Nelson, C. H., & Whittle, M. 1995, ApJS, 99, 67 (Paper I)
Oliva, E., Origlia, L., Kotilainen, J. K., & Moorwood, A. F. M. 1995, A&A, in press
Phillips, M. M., Charles, P. A., & Baldwin, J. A. 1983, ApJ, 266, 485
Phillips, M. M., Jenkins, C. R., Dopita, M. A., Sadler, E. M., & Binette, L. 1986, AJ, 91, 1062
Rodríguez-Espinosa, J. M., Rudy, R. J., & Jones, B. 1987, ApJ, 312, 555
Sadler, E. M., Jenkins, C. R., & Kotanyi, C. G. 1989, MNRAS, 240, 591
Shuder, J. M. 1981, ApJ, 244, 12
Simien, F., & de Vaucouleurs, G. 1986, ApJ, 302, 564
Smith, E. P., Heckman, T. M., & Illingworth, G. D. 1990, ApJ, 356, 399
Terlevich, E., Diaz, A. I., & Terlevich, R. 1990, MNRAS, 242, 271
Tonry, J. 1981, ApJ 251, L1
Tonry, J., & Davis, M. 1979, AJ, 84, 1511
Ulvestad, J. S., & Wilson, A. S. 1984a, ApJ, 278, 544
———. 1984b, ApJ, 285, 439
———. 1989, ApJ, 343, 659
Veilleux, S. 1991a, ApJ, 369, 331
———. 1991b, ApJS, 75, 383
Whitmore, B. C., & Kirshner, R. P. 1981, ApJ, 250, 43
Whittle, M. 1985a, MNRAS, 213, 1
———. 1985b, MNRAS, 213, 33
———. 1992a, ApJS, 79, 49 (W92a)
———. 1992b, ApJ, 387, 109 (W92b)
———. 1992c, ApJ, 387 121 (W92c)
———. 1992d, in AIP Conf. Proc. 254, Testing the AGN Paradigm, ed. S. S. Holt, S. G. Neff, & C. M. Urry (New York: AIP), 607
Whittle, M., Pedlar, A., Meurs, E. J. A., Unger, S. W., Axon, D. J., & Ward, M. J. 1988, ApJ, 326, 125
Wilson, A. S., & Heckman, T. M. 1985, in Astrophysics of Active Galaxies and Quasi-Stellar Objects, ed. J. S. Miller (Mill Valley: University Science), 39
Wilson, A. S., & Willis, A. G. 1980, ApJ, 240, 429
Yee, H. K. C. 1980, ApJ, 241, 894
Zasov, A. V., & Dibai, E. A. 1970, Astrofizika, 47, 23
Zasov, A. V., & Lyuti, V. M. 1973, Astrofizika, 50, 253
———. 1981, AZh Pis'ma, 7, 459
Zasov, A. V., & Niezvestny, S. I. 1989, AZh Pis'ma, 15, 963
Zirbel, E. L., & Baum, S. A. 1995, ApJ 448, 548